APCC
APEC CLIMATE CENTER

PREFACE

It is our pleasure to present to you the APEC Climate Center (APCC)'s Technical Report 2011, which reports the core outcomes of our research activities from the past year.

Since 2005, APCC, as a hub of climate information in the Asia-Pacific region, has strived to share our analysis and prediction of abnormal climate and to apply this information to regional development. The center has established the largest Multi-Model Ensemble (MME) system for seasonal prediction through its international science network and has provided value-added products to various stakeholders. Recently, APCC has expanded its mandate to include enhancement of the capacity of APEC member economies information to respond effectively to climate change and variability through better application of climate.

To achieve its research and social objectives, in 2011, APCC made efforts to research improvements in its climate prediction performance from various angles and towards better understanding of climate variability and the reproducibility of the climate models for the relevant application of climate information to society. The following technical report provides more information about our research outcomes from 2011.

APCC will continue to improve the quality and accuracy of climate information, recognizing that the utility of this information is only as good as its quality. We would like to make the best use of our research results for the benefit of society and academia. We also welcome any feedback on this report or on our services.

My best and warmest regards to all of you.

Dr. Chin-Seung Chung
Director/APEC Climate Center

CONTENTS

Evaluation and Future Projection of Changes in Extreme Temperature and Precipitation Events in the Asia-Pacific Region Using AOGCMs

■■ Dr. Ok-Yeon Kim

APCC
TECHNICAL REPORT 2011-03

Evaluation and Future Projection of Changes in Extreme Temperature and Precipitation Events in the Asia-Pacific Region Using AOGCMs

Dr. Ok-Yeon Kim

ABSTRACT

This study examined the performance of global climate models in representing observed spatial and temporal patterns of climate extremes and inspected the projection of climate extremes in the Asia-Pacific region under a future warmer climate scenario. For the last few decades, observations show considerable warming of temperature extremes in high-topographic regions such as the eastern part of Northern Asia (NAS), the Tibetan Plateau (TIB), and East Asia (EAS), whereas models simulate weaker warming in the same regions. Models simulate more warming in sub-tropical regions such as South Asia (SAS), the western part of East Asia (EAS) and Northern Australia (NAU). Observations reveal increasing trends in annual total precipitation in wet days, very wet days, and extremely wet days, especially in Northern Asia (NAS), South Asia (SAS), Northern Australia (NAU) and Southern Australia (SAU), whereas models fail to capture such trends in precipitation extremes over the same regions.

Under the projected future climate, asymmetric extreme events are expected to arise in the late 21st century. The annual number of warm extreme events (TX90p and TN90p) is expected to increase more, and with greater variance, than is the number of cool extreme events (TX10p and TN10p). It is expected that tropical regions (South Asia (SAS), Indochina, Southeast Asia (SEA), and Northern Australia (NAU)) may possibly make a more considerable contribution to the large median increase in projected warm events than other regions at higher latitudes, and the larger variance of warm events may possibly be attributable to the increase in temperature extreme variability in South Asia (SAS) and Northern Australia (NAU). Increasing trends in warm extremes are expected to be large, especially in South Asia (SAS), Southeast Asia (SEA), and Northern Australia (NAU), and those regions are expected to experience more frequent and long-lasting warm spells. Based on the projected changes in precipitation extremes, many regions located in South Asia (SAS), East Asia (SEA), Southeast Asia (SEA) and Northern Asia (NAS) may be expected to undergo heavy precipitation extremes in the future climate. The fraction of annual high precipitation amounts due to very wet days (R95pTOT) and extremely wet days (R99pTOT) is expected to increase substantially over those regions.

1. INTRODUCTION

1.1 Background

The last Intergovernmental Panel on Climate Change (IPCC) Assessment Report (AR) Synthesis Report (2007a; 2007b) defines an *extreme weather event* as “An event that is rare at a particular place and time of year. Definitions of “rare” vary, but

an extreme weather event would normally be as rare as or rather than the 10th or 90th percentile of the observed probability density function. By definition, the characteristics of what is called extreme weather may vary from place to place in an absolute sense. Single extreme events cannot be simply and directly attributed to anthropogenic climate change, as there is always a finite chance the event in question might have occurred naturally. When a pattern of extreme weather persists for some time, such as a season, it may be classed as an *extreme climate event*, especially if it yields an average or total that is itself extreme (e.g., drought or heavy rainfall over a season)." The assessment report mentioned that climate change may be perceived most through the impacts of extreme events, such as cold and heat waves, drought or floods. It also reported that there is increasing confidence that some extremes will become more frequent, more widespread and more intense during the 21st century (IPCC, 2007a; 2007b).

It has been well established that climate variability will depend more on changes in the intensity and frequency of extreme events than on changes in the mean climate (e.g., Lynch and Brunner, 2007). Moreover, it has also been posited that the largest changes in climate under enhanced greenhouse gas conditions are likely to be manifested as extreme events (Houghton et al. 2001). Assertions regarding the importance of climate extremes have drawn attention to studies on the change and projection of climate extremes in various geographies. Characteristics of changes in climate extremes have been examined during the past several years using historical station observations (e.g., Easterling et al., 2000; Frich et al., 2002; Klein Tank and Können, 2003; Moberg and Jones, 2005; Alexander et al., 2006; Caesar and Alexander et al., 2006; Coelho et al., 2008; Choi et al., 2009; Caesar et al., 2010; Kioutsioukis et al., 2010). In addition to these observational studies, climate extremes have been projected for many regions over the globe by employing global climate models component to the Coupled Model Intercomparison Project phase 3, which formed the basis of the Fourth Assessment of the IPCC (e.g., Kiktev et al., 2003; Tebaldi et al., 2006; Kharin et al., 2007; Sillmann and Roeckner, 2008; Alexander and Arblaster, 2009; Marengo et al., 2010; Rusticucci et al., 2010; Im et al., 2011). The results of these studies indicate that warming trends appear to be clear in observations made over the last few decades, and those warming trends are expected to increase

in intensity under projected future climate conditions. The spatial extents of warming trends appear to vary from region to region under the current climate, but the increased likelihood of extreme weather events associated with warmer extreme temperatures may be expected globally under the future climate. Climate extremes related to precipitation are found to have rather diverse features from area to area. For example, there is no consensus regarding the simulations of changes in regional precipitation under the projected future warming climate (IPCC, 2007a). This is problematic because regional impacts induced by precipitation extremes could greatly affect many environments including ecosystems and vulnerable human societies (IPCC, 2007b).

As mentioned above, a number of studies have attempted to identify the predictive skill of global climate models in simulating daily extreme climate values. Past studies show that global climate models are unable to reproduce observed quantities or rates of change due to the relatively coarse resolutions of atmosphere-ocean coupled general circulation models (AOGCMs), and because the gridboxes typical among global models have problems of aggregation and interpolation of locally-recorded extreme events (Alexander and Arblaster, 2009; Chen et al., 2010; Hegerl et al., 2004; Kiktev et al., 2003; Tebaldi et al., 2006; Tebaldi and Knutti, 2007). In general, changes in moderately extreme temperature appear robust and similar among global models, while climate change patterns for precipitation appear to be highly model dependent, as evidenced by the low correlations between modeled climate change patterns (Alexander and Arblaster, 2009; Hegerl et al., 2004; Tebaldi et al., 2006). According to the study of Tebaldi et al. (2006), the consensus and significance of precipitation intensity appear to be weaker among AOGCMs when regional patterns are considered. Also, while global model simulations tend to resolve observed patterns of temperature variability fairly well, they tend to poorly reproduce observed trends in precipitation (Kiktev et al., 2003). Despite the uncertainties and limitations of global model-driven data in diagnosing daily climate extremes, the use of global climate models has enabled us to make general statements in terms of historical and projected daily climate extremes, especially regarding temperature, and to understand future patterns of climate extremes (e.g., Emori and Brown, 2005; Meehl et al., 2005; Räisänen, 2005). That is, advances in global climate model performance have enabled scientists to

simulate mean values and variability of atmospheric extreme events (Marengo et al. 2010; Rusticucci, 2010). Alexander et al. (2009) mentioned that no single model is superior or inferior in representing the observed trends and patterns in extreme temperature events. In addition, the uncertainty of the internal variability of climate change simulations from a single climate model is much smaller than that between different models (Deque et al., 2005). Since the representation and projection in this study are derived from several global climate models (four in total in this study), we may be able to consider the systematic errors inherent in the individual models and their influence on the climate features represented in the trend analysis herein.

> ***Has there been a change in extreme events like heat waves, droughts, floods, and hurricanes?***
> (IPCC, *Climate Change 2007: The Physical Science Basis*, *Frequently Asked Question 3.3*):
> "Since 1950, the number of heat waves has increased and widespread increases have occurred in the numbers of warm nights. The extent of regions affected by droughts has also increased as precipitation over land has marginally decreased while evaporation has increased due to warmer conditions. Generally, numbers of heavy daily precipitation events that lead to flooding have increased, but not everywhere. Tropical storm and hurricane frequencies vary considerably from year to year, but evidence suggests substantial increases in intensity and duration since the 1970s. In the extratropics, variations in tracks and intensity of storms reflect variations in major features of the atmospheric circulation, such as the North Atlantic Oscillation."

1.2 Purpose of the study

Studies on the identification of climate extreme events have been carried out through two major approaches. One of them is to use a set of core indices of extremes which considers the intensity, frequency, and duration of extremes. Extreme indices describe in general moderate and statistically robust extremes which are meant to be easily understandable and applicable for model comparison as well as for climate impact studies (e.g., Alexander and Arblaster, 2009; Im et al., 2011; Kiktev et al., 2003; Klein Tank and Konnen, 2003; Sen Roy and Balling, 2004; Sillmann and Roeckner, 2008; Tebaldi et al., 2006). The Joint World Meteorological Organization Commission for Climatology (CCl)/World Climate Research Programme (WCRP) project on Climate Variability and Predictability (CLIVAR) Expert Team on Climate Change Detection, Monitoring and Indices (ETCCDMI)[1] developed a suite of climate change indices.

1) See Appendix A: Name and definitions of a suite of climate change indices

Another approach for understanding climate extremes is to apply statistical modeling of extreme values. Several parametric approaches, including Generalized Extreme Value (GEV) distribution or Generalized Pareto (GP) distribution, characterize the distribution of extreme events and simplify them to estimate return values and return levels of their annual extremes (e.g., Coelho et al., 2008; Kharin et al., 2007; Kioutsioukis et al., 2010; Sillmann and Croci-Maspoli, 2009).

In this study, we will focus on the changes in climate extremes in the Asia-Pacific region as shown in Fig. 1. According to the IPCC (2007a), relative to global mean warming (mean warming between 1980 to 1999 and 2080 to 2099 of 2.5°C), warming is expected to be similar to the global mean in Southeast Asia, somewhat greater in South Asia (3.3°C) and East Asia (3.3°C), and much greater in the continental interior of Asia (3.7°C in central Asia, 3.8°C in Tibet and 4.3 oC in northern Asia). Regarding precipitation mean changes, an increase in annual precipitation is expected in most of Asia, and most models show the percentage increase being largest and most consistent in North and East Asia. Exceptionally, a decrease in mean precipitation is expected in central Asia. While broad aspects of Asian climate change show consistency among AOGCM simulations, a number of sources of uncertainty remain. A lack of observational data in some areas limits model assessment (IPCC, 2007a). It is also likely that some local climate changes will vary significantly due to regional trends associated with the region's very complex topography and marine influences (IPCC, 2007a). Because of this complexity, there has been little assessment of the projected changes in regional climate means and extremes in the Asia region (IPCC, 2007a). This study would be the first attempt to address observed and modeled extreme projections for an Asia-Pacific domain.

Using climate extreme indices, this study seeks to answer two scientific questions: 1) how spatial and temporal trends in temperature and precipitation extremes are changing in the present climate and whether global climate models are able to adequately reproduce the observed patterns of climate extremes (section 3.1), and 2) what changes in trends in climate extremes can be expected under the projected future climate change (section 3.2).

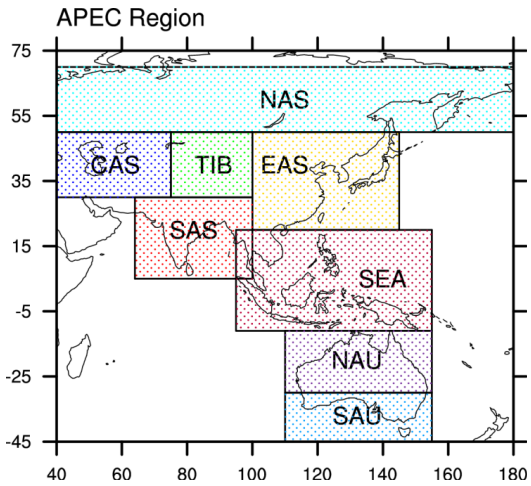

Figure 1 Domain of the Asia-Pacific (APEC) region. Region classification is followed by suggestions in the IPCC AR4 (2007a): Northern Asia (NAS), Central Asia (CAS), Tibetan Plateau (TIB), East Asia (EAS), South Asia (SAS), Southeast Asia (SEA), Northern Australia (NAU), and Southern Australia (SAU).

2. METHODOLOGY

2.1 Model and experiments

The model-based climate extreme indices used in this study are calculated from four coupled AOGCMs including MRI-CGCM2.3.2 (Yukimoto et al., 2001; Yukimoto and Noda, 2002), CSIRO-MK3.0 (Gordon et al., 2002), NIES-MIROC3.2-hires (Hasumi et al., 2004), and ECHAM5/MPI-OM (Roeckner et al., 2003), which participate in the Program for Climate Model Diagnosis and Intercomparison (PCMDI; http://www-pcmdi.llnl.gov/) in support of the IPCC AR4. The utilization of several models enables us to take into account and balance out systematic errors in the models (Deque, 2005). Model experiments used in this study include simulations of the twentieth century climate (20C3M) in which the forcing agents are taken from historical records of greenhouse gases, sulfate aerosol direct effects, volcanoes and solar forcing. For the future scenario experiments, forcing agents of the experiments such as greenhouse gases and sulfate aerosol direct effects are prescribed

according to the characteristics of three different scenarios, A1B, A2 and B1 in the IPCC Special Report on Emission Scenarios (SRES; Nakicenovic et al., 2000).

2.2 Climate extreme indices

A set of indices for climate extremes, which is calculated using time series of daily temperature and precipitation data, is used to analyze the temporal and spatial trends in climate extremes and to compare observed and simulated extremes. Extreme indices are defined by the Expert Team on Climate Change Detection Monitoring and Indices (ETCCDMI), a team jointly sponsored by the World Meteorological Organization (WMO) Commissions of Climatology (CCI) and the Climate Variability and Predictability (CLIVAR) project (Peterson, 2005).

Since CLIVAR provides the software packages for calculating extremes indices, we modified and used the packages to allow the calculation of indices with gridded model data. The indices for climate extremes are calculated on an annual basis for each of the global climate models and ensemble averages are taken from the 20C3M and three different scenario simulations. For comparison of model and observation-based indices in the present climate (20C3M), the observed climate extremes, called the HadEX dataset, are used to represent observed data. The dataset includes various indices representing many aspects of extreme events, and the indices are calculated on the basis of a worldwide weather observational dataset from the Hadley Centre based in the United Kingdom (Alexander et al., 2006). Those indices are calculated at a horizontal resolution of 3.75 degrees longitude by 2.5 degrees latitude over the period of 1951 to 2001. A total of 27 indices are considered to be core indices (e.g., Sillmann and Roeckner, 2008), but only a few indices are selected and analyzed in this study based on the following criteria. Indices for temperature and precipitation extremes have to be statistically robust with fairly short return periods. This indicates that high occurrence of extreme events will likely allow significant trend analysis (Im et al., 2011). In addition, the indices analyzed in this study potentially reflect many aspects of a changing climate, thus the information estimated from the indices should be meaningful for additional studies on climate

change impacts. Note also that some indices are calculated in seasonal or monthly timescales; however, sub-annual specification is not considered in this study.

Tables 1 and 2 describe the abbreviations and definitions of the climate extreme indices used in this study, which include ten temperature-based indices and eight precipitation-based indices. Temperature extreme indices such as summer days (SU), tropical nights (TR), icing days (ID), and frost days (FR) are defined as the number of days exceeding (or falling below) a critical value, and these are the simplest quantitative indications of a change in the frequency distribution of the maximum and minimum temperature. The four temperature extreme indices are classified as absolute threshold-based indices. Percentile-based indices are also considered for analyzing changes in the tail thickness of the temperature distribution. Cool and warm days (TX10p and TX90p) and nights (TN10p and TN90p) are included in the percentile-based indices. A warm spell duration index is also used to consider the duration properties of maximum temperature indicating the intensity of heat stress during hot period. As an additional and important climate change variable related to temperature, diurnal temperature range (DTR) is also considered. Changes in DTR may partially explain the proportion of local effects due to urban growth, desertification, and variation in local land use from the aspects of maximum and minimum temperature behavior in the region of interest (Easterling et al., 1997).

As simply quantified precipitation indices, monthly maximum 1-day precipitation amounts (RX1day), simple precipitation intensity (SDII), and number of heavy precipitation days (R10mm) are used. Annual total precipitation in wet days (PRCPTOT) plus total precipitation in very wet days (R95pTOT) and extremely wet days (R99pTOT) are also considered. The indices based on either 95^{th} or 99^{th} percentile are regarded as good indicators for changes in the upper tail thickness of the heavy precipitation distribution. Also used are consecutive dry days (CDD) and consecutive wet days (CWD), which are related to the likelihood of occurrence of floods or drought.

Table 1 Abbreviations and definitions of the extreme temperature climate indices used in this study

Abbreviation(unit)	Name	Definition
SU(days)	Summer days	Annual count of days when $T_{max} > 25°C$
TR(days)	Tropical nights	Annual count of days when $T_{min} > 20°C$
ID(days)	Icing days	Annual count of days when $T_{max} < 0°C$
FD(days)	Frost days	Annual count of days when $T_{min} < 0°C$
TN10p(%)	Cool nights*	Percentage of days when $T_{min} < 10^{th}$ percentile
TX10p(%)	Cool days*	Percentage of days when $T_{max} < 10^{th}$ percentile
TN90p(%)	Warm nights*	Percentage of days when $T_{min} > 90^{th}$ percentile
TX90p(%)	Warm days*	Percentage of days when $T_{max} > 90^{th}$ percentile
WSDI(days)	Warm spell duration*	Annual count of days with at least 6 consecutive days when $T_{max} > 90^{th}$ percentile
DTR(oC)	Diurnal temperature Range	Monthly mean difference between T_{max} and T_{min}

* The percentage of temperature is calculated for the base period of 1961-1990

Table 2 Abbreviations and definitions of the extreme precipitation climate indices used in this study

Abbreviation(unit)	Name	Definition
RX1day(mm)	Monthly maximum 1-day precipitation amount	Monthly maximum 1-day precipitation
SDII(mm/day)	Simple precipitation intensity	Daily precipitation amount on wet days (>1mm) divided by the number of wet days
R10mm(days)	Number of heavy precipitation days	Annual count of days when PRCP ≥ 10mm
PRCPTOT(mm)	Annual total precipitation in wet days	Annual total precipitation
R95pTOT(mm)	Annual total precipitation in very wet days*	Annual total precipitation when PRCP > 95^{th} percentile
R99pTOT(mm)	Annual total precipitation in extremely wet days*	Annual total precipitation when PRCP > 99^{th} percentile
CDD(days)	Consecutive dry days	Maximum number of consecutive days with PRCP < 1mm
CWD(days)	Consecutive wet days	Maximum number of consecutive days with PRCP ≥ 1mm

* The percentage of precipitation is calculated for the base period of 1961-1990

2.3 Temporal and spatial trend analysis

Each of the ensemble runs for the present (20C3M) and projected future climate (SRES) is interpolated onto the HadEX data grid and then the model-based indices

for climate extremes are calculated at the interpolated model grids. The time-dependent masking of missing grid values in the HadEX dataset is also applied to the model-based indices when calculating the time series and trends. The time series for each of the indices are calculated by averaging the masked grid boxes within the area encompassing 30°S–40°N and 50°E–180°E. This helps us compare the magnitude and interannual variability of the observed and simulated extremes. In addition to the time series, trends in temperature and precipitation extreme indices are calculated between 1961 and 2000 for present climate comparison for each grid box. Trends are only calculated in grid boxes where all 40-years of observed indices exist. For each of the indices, trends are calculated using the ordinary least squares (OLS) regression method. Alexander and Arblaster (2009) showed OLS regression to be computationally efficient.

OLS is one of the first regression methods for estimating the unknown parameters in a linear regression model. It is a technique to understand a relationship between a dependent and an independent variable. If we plot n observations Y_i and X_i (i=1,2 ,⋯,n) on a dependent variable Y and an independent variable X in a scatter plot, then points (X_i,Y_i) will not track any straight line (1) due to the omission of variables that affect Y,

$$Y = \alpha + \beta X \tag{1}$$

and the contribution of omitted variables to Y is the residual u written in (2).

$$u = Y - \alpha - \beta X \tag{2}$$

Then, how do we find the hidden straight line if there are omitted variables? We first use the ordinary least squares method, which computes residuals for i=1,2,⋯,n as in (3).

$$u_i = Y_i - \alpha - \beta X_i \tag{3}$$

Second, we compute the sum of squared residuals as in (4).

$$S(\alpha, \beta) = \sum_{i=1}^{n} u_i^2 = \sum_{i=1}^{n} (Y_i - \alpha - \beta {X_i}^2) \tag{4}$$

The sum of squared residuals in (4) depends on the coefficients α and β, and the OLS solution can be found by minimizing $S(\alpha, \beta)$ with respect to α and β. Finally, the OLS solution is shown as (5).

$$\begin{aligned} S(\alpha,\beta) &= \sum_{i=1}^{n}(Y_i - \alpha - \beta X_i)^2 \\ &= \sum_{i=1}^{n}(Y_i^2 + \alpha^2 + \beta^2 X_i^2 - 2\alpha Y_i - 2\beta X_i Y_i + 2\alpha\beta X_i) \\ &= \sum_{i=1}^{n} Y_i^2 + n\alpha^2 + \beta^2 \sum_{i=1}^{n} X_i^2 - 2\alpha \sum_{i=1}^{n} Y_i - 2\beta \sum_{i=1}^{n} X_i Y_i + 2\alpha\beta \sum_{i=1}^{n} X_i \end{aligned} \quad (5)$$

This is a quadratic function in α and β. Now we have the slopes in the α- and β-directions. There are the partial derivatives with respect to α and β. $S(\alpha, \beta)$ is the minimum at the value of (α, β) where the slope in both directions is 0. By setting two partial derivatives equal to 0, two linear equations in two unknowns $\hat{\alpha}$ and $\hat{\beta}$ can be solved. Then, the values of $\hat{\alpha}$ and $\hat{\beta}$ that minimize the sum of squared residuals can be obtained in (6).

$$\begin{aligned} \hat{\beta} &= \frac{\sum_{i=1}^{n}(X_i - \overline{X})(Y_i - \overline{Y})}{\sum_{i=1}^{n}(X_i - \overline{X})^2} \\ \hat{\alpha} &= \overline{Y} - \hat{\beta}\overline{X} \end{aligned} \quad (6)$$

These are the Ordinary Least Squares (OLS) solutions to the problem of fitting a straight line to the points in a scatter plot. The least squares line in (7) is the straight line that best 'fits' the scatter plot.

$$\overline{Y} = \hat{\alpha} + \hat{\beta}\overline{X} \quad (7)$$

Also, a trend remains unchanged irrespective of the trend calculation method. For investigation of trend significance, a non-parametric Mann-Kendall test (Kendall, 1975; Mann, 1946) is carried out at the 10%, 5% and 1% significance levels. The Mann-Kendall test compares the relative magnitudes of sample data rather than the data themselves (Gilbert, 1987). The test has several advantages, the first of which is that the test needs not assume that the data conform to any specific parametric distribution. In addition, it can also deal with missing data by assigning them a common value that is smaller than the smallest measured value in the dataset. A very high

positive value of the Mann-Kendall statistic indicates a significantly increasing trend, whereas a very low negative value is a sign of a significantly decreasing trend.

Kendall (1975) describes a normal-approximation test that could be used for datasets with more than 10 values, provided there are not many inherent tied values. First, the data values are evaluated as an ordered time series. Each data value is then compared to all subsequent data values. The initial value of the Mann-Kendall statistic, S is assumed to be 0 which means there is no trend. If a data value from a later time period is higher than a data value from an earlier time period, S is incremented by 1. On the other hand, if the data value from a later time period is lower than an earlier sampled data value, S is decremented by 1. The aggregate result of all such increments and decrements yields the final value of S. The Mann-Kendall statistic S is given by

$$S = \sum_{i=1}^{n-1} \sum_{j=i+1}^{n} \text{sign}(x_j - x_i) \tag{8}$$

where x_1, x_2, x_3,$\cdots$.x_n represent n sequential data values where x_i represents the data value at time i, and sign(x_j-x_i) is assumed as

$$\begin{aligned} \text{sign}(x_j - x_i) &= 1 \quad \text{if } x_j - x_i > 0 \\ &= 0 \quad \text{if } x_j - x_i = 0 \\ &= -1 \quad \text{if } x_j - x_i < 0 \end{aligned} \tag{9}$$

A very high positive value of S is an indicator of an increasing trend, and a very low negative value indicates a decreasing trend. However, it is necessary to compute the probability associated with S and the sample size, n, to statistically quantify the significance of the trend. The variance of S, VAR(S) is also computed by the following equation (10),

$$\text{VAR}(S) = \frac{1}{18}\left[n(n-1)(2n+5) - \sum_{i=1}^{k} e_i(e_i - 1)(2e_i + 5)\right] \tag{10}$$

where n is the number of data points, k is the number of tied groups (a tied group is a set of sample data having the same value), and e_i is the size of the i^{th} tied group. S is expected to have a normal distribution with mean 0 and variance S with the null hypothesis H_0 that there is no trend displayed by the time series

(Im et al. 2011). Next, the Mann-Kendall statistic Z (a normalized test statistic) is computed as follows,

$$Z = \frac{S-1}{\sqrt{VAR(S)}} \quad \text{if} \quad S > 0$$
$$Z = 0 \quad \text{if} \, S = 0$$
$$Z = \frac{S+1}{\sqrt{VAR(S)}} \quad \text{if} \quad S < 0 \tag{11}$$

where Z is a standard normal variable. The probability associated with this normalized test statistic is then computed. The probability density function for a normal distribution with a mean 0 and a standard deviation of 1 is given by the following equation,

$$f(z) = \frac{1}{\sqrt{2\pi}} e^{-\frac{1}{2}z^2} \tag{12}$$

The hull hypothesis H0 showing that Z is not statistically significant (i.e., there is no significant trend) with α significance level is accepted if $-Z_{1-\alpha/2} \leq Z \leq Z_{1-\alpha/2}$. The alternative hypothesis H1 indicating that Z is statistically significant (i.e., there is a significant trend) with α significance level is accepted $Z < -Z_{1-\alpha/2}$ or if $Z > Z_{1-\alpha/2}$.

3. RESULTS

3.1 Comparison between observed and simulated extremes over the Asia-Pacific region

3.1.1 Temperature extremes

Spatial trends across the Asia-Pacific (APEC) region are examined in Fig. 2. Compared with the observed spatial trend patterns of the temperature extreme indices, the global models are generally able to capture the magnitude and significance of spatial trend patterns of the corresponding indices. The significant observed patterns

of increasing trends in summer days (Fig. 2(a)) and tropical nights (Fig. 2(b)) are well simulated in the 20C3M experiments (Figs. 2(k)-(l)) excepting for the Tibetan Plateau (TIB). The numbers of summer days and tropical nights tend to increase, especially in Central Asia (CAS), inland East Asia (EAS) and Northern Australia (NAU). Comparing Figs. 2(a)-(b) and Figs. 2(k)-(l), it is also noticeable that the warming trends shown by the models appear much weaker than the observed trends in the Tibetan Plateau (TIB). This is due to either the pre-defined absolute threshold used to define the indices or temperature underestimation (i.e., cold biases) in the GCMs. More specifically, GCMs tend to underestimate temperature, especially in high topographic regions, due to an overestimation of snow-ice albedo or a deficiency in the calculation of surface heat flux on ice in the models (IPCC, 2007a; Mao and Robock, 1998). The cold biases in the GCMs therefore affect the representation of warmer extreme indices (i.e., summer days and tropical nights). Careful consideration of this aspect is needed for model-based temperature extreme projections. With regard to icing days (Fig. 2(c)-(m)) and frost days (Fig. 2(d)-(n)), warming trends (i.e., decreasing trends) in those indices appear weaker in models than in observations in the eastern part of Northern Asia (NAS), the Tibetan Plateau (TIB), and some parts of East Asia (EAS). It may also be related to the models' difficulty in simulating the effects of the dramatic topographic relief, as well as the distorted albedo feedbacks due to extensive snow cover (IPCC, 2007a).

It is shown from Fig. 2 that models also well capture the overall aspects of the magnitude of trends in all percentile-based indices. In other words, models are capable of simulating the magnitude of change in the tail thicknesses of minimum and maximum temperature-related indices. It is worth mentioning that the sign of the significant simulated trends in those indices is consistent with the sign of the observed trends across the region considered in this study. Considering a regional perspective, observed decreases (increases) in the lower (upper) tails tend to be large in the eastern part of Northern Asia (NAS), the Tibetan Plateau (TIB), and East Asia (EAS) (Fig. 2(e)-(h)). Meanwhile, simulated decreases (increases) in the lower (upper) tails tend to be large in South Asia (SAS), the western part of East Asia (EAS) and Northern Australia (NAU). This suggests that the observed warming in percentile-based temperature extremes tends to be large in the high-topographic

regions (i.e., the eastern part of Northern Asia (NAS), the Tibetan Plateau (TIB), and East Asia (EAS)). Meanwhile, models are very likely to simulate large warming in the sub-tropical regions (i.e., South Asia (SAS), the western part of East Asia (EAS) and Northern Australia (NAU)). In part, it is also related to the models' lack of representation of complex topography and the associated mesoscale weather systems of the high-altitude and arid areas (IPCC, 2007a).

In terms of the magnitude of changes in the lower/upper tails of the probability distribution of temperature, comparison of observed changes in the lower tails of the probability distributions of minimum temperature (cool nights, Fig. 2(e)) and maximum temperature (cool days, Fig. 2(f)) reveals decreasing trends (i.e., thinner lower tails) in the minimum temperature-related indices compared to those in the maximum temperature-related indices. This is also the case for the upper tails. Increasing trends (i.e., thicker upper tails) are also stronger in minimum temperature indices (warm nights, Fig. 2(g)) compared to maximum temperature indices (warm days, Fig. 2(h)) in observations. As shown in observation, the global models also better exhibit the thinner and thicker lower and upper tails of the minimum temperature-related indices, respectively, than those of the maximum temperature -related indices (Figs. 2(o)-(r)). However, differences in the modeled magnitude of trends in the tails of the probability distributions of minimum and maximum temperature appear smaller than those in the observed magnitude of trends. This fact leads to almost insignificant diurnal temperature range (DTR) trends in model simulations (Fig. 2(t)) compared to observations (Fig. 2(j)). Comparison of observed and simulated warm spell duration indices (Figs. 2(i) and 2(s)) reveals that models simulate large increasing changes in the western part of Northern Asia (NAS), Central Asia (CAS), and the Yangtze River basin in China. Except for the Yangtze River basin, the models well simulate the increasing trends shown by observations.

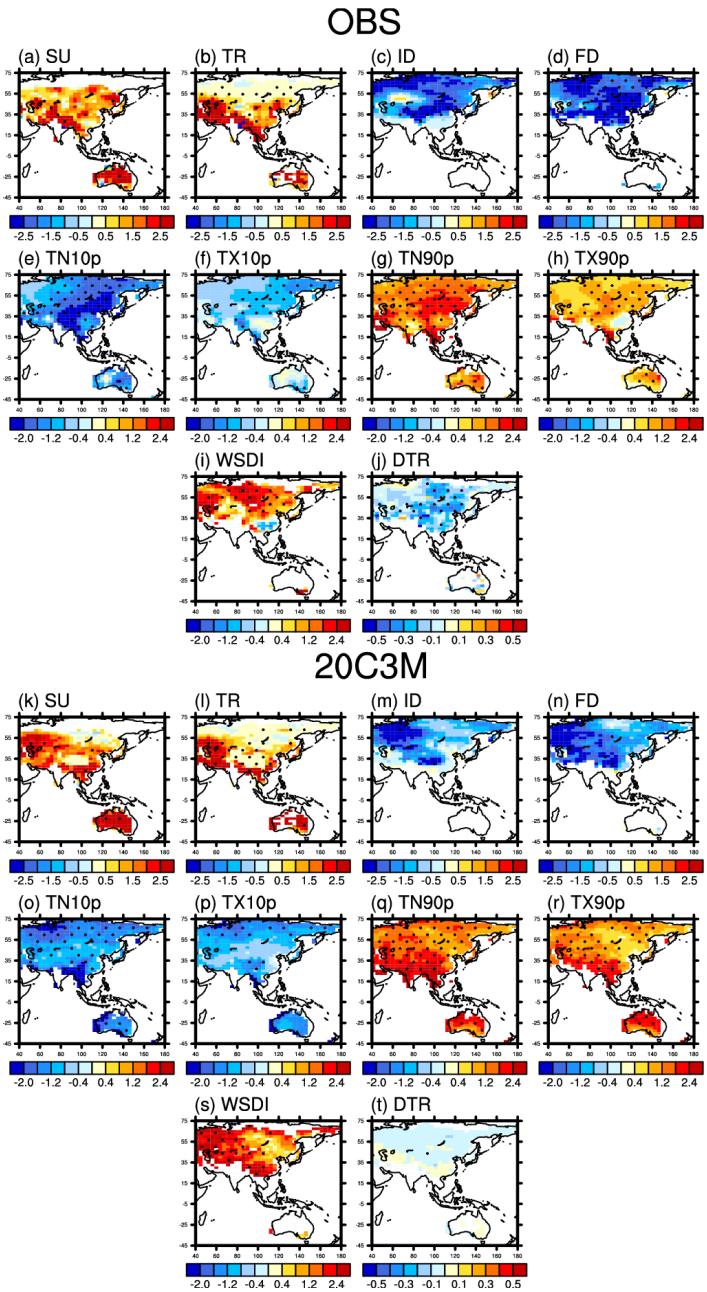

Figure 2 Observed (upper two panels, OBS) and simulated (lower two panels, 20C3M – averages for four model simulations) decadal spatial trends in temperature extremes calculated between 1961 and 2000 over the Asia-Pacific (APEC) region. Model data are masked out with grid boxes which have observations. Stippling indicates the trend is significant at the 0.05 level.

The time series for each of the temperature indices calculated from observations indicates clear warming trends which are well represented in model simulations with the exception of diurnal temperature range (Fig. 3, averaged over the whole Asia-Pacific (APEC) region). As threshold-based extreme indices, increasing trends in summer days (Fig. 3(a)) and tropical nights (Fig. 3(b)) and decreasing trends in icing days (Fig. 3(c)) and frost days (Fig. 3(d)) all indicate warming trends both in observations and in model simulations. Even though the magnitude of simulated trends in threshold-based indices is somewhat departed from the observed trends, the overall observed year-to-year variability of temperature extremes is comparable to the variability of model simulated extremes. Note that correlation coefficients of four threshold-based indices (summer days, tropical nights, icing days and frost days) between the models and observations are about 0.86, 0.94, 0.34 and 0.78, which are all statistically significant at a 0.05 significance level. This indicates that simulated magnitudes of frequency behavior of maximum and minimum temperature have uncertainty, but that their temporal trend and variability are relatively reliable.

The percentile-based indices also indicate warming trends, as do the threshold-based indices. From the percentile-based indices, the observed trends agree reasonably well with the simulated trends, which implies that model simulations succeed in capturing the temporal changes in the thickness of the upper or lower tails of the probability distributions of the maximum and minimum temperatures in the Asia-Pacific (APEC) region. The decreasing trends in the lower tails (cool nights, Fig. 3(e) and cool days, Fig. 3(f)) and increasing trends in the upper tails (warm nights, Fig. 3(g) and warm days, Fig. 3(h)) both indicate an increase in the intensity of extreme events, specifically for warm extremes. Choi et al. (2009) found the similar result, observing that the annual frequency of cool nights (days) has decreased and the frequency of warm nights (days) has increased on average over the Asia-Pacific Network region for the period of 1955-2007. As for interannual variability of percentile-based indices, minimum temperature-related percentile-based indices show higher correlation (0.75 in Fig. 3(e) and 0.81 in Fig. 3(g)) than maximum temperature-related indices (0.52 in Fig. 3(f) and 0.63 in Fig. 3(h)), but all are statistically significant at the 0.05 significance level.

In terms of duration properties as depicted in Fig. 3(i), observed increasing trends

in warm spell duration have become more apparent since the early 1990s (Alexander et al., 2006), and model simulations exhibit similar increasing trends. The correlation coefficient of warm spell duration index (WSDI) is relatively moderate (0.68), but is statistically significant at a 0.05 significance level.

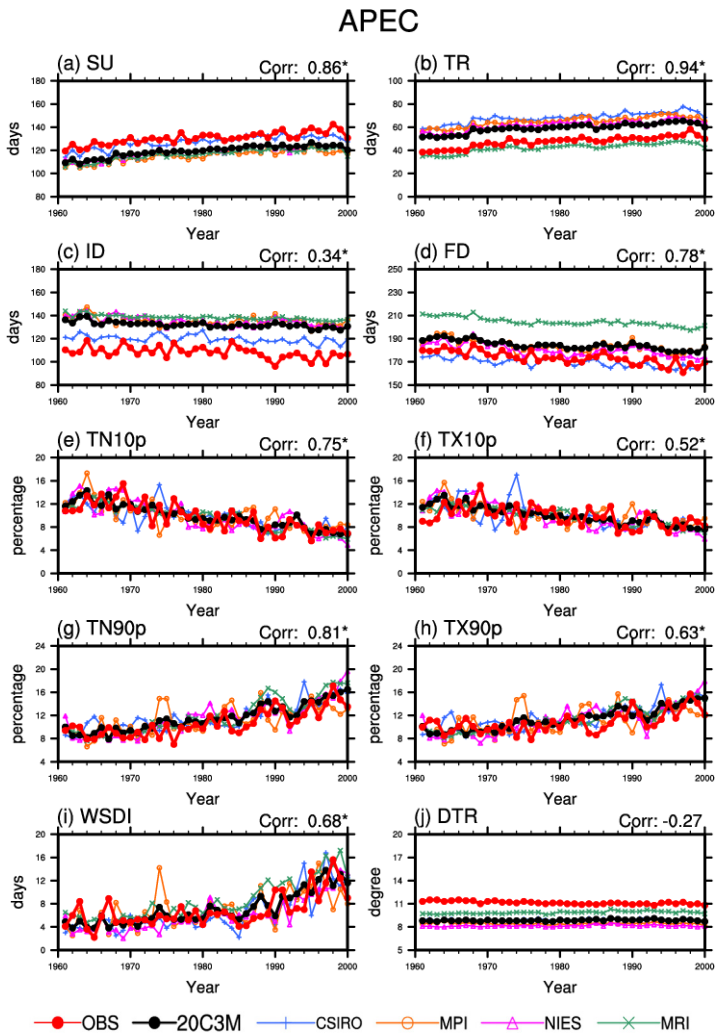

Figure 3 Temporal trends in temperature extremes: the indices for temperature extremes are averaged over the Asia-Pacific (APEC) region for the current climate period (1961-2000). The thick black and red lines indicate the model simulations (20C3M – averages for four model simulations) and the observation (OBS), respectively. The thin colored lines with small symbols indicate each model simulation. Correlations between 20C3M and OBS and their significance tests (asterisk: significant at the 0.05 significance level) are also given.

Fig. 3(j) exhibits slightly decreasing trends in the diurnal temperature range (DTR) from observed temperature that appear to be inconsistent with those from model simulations. The observed and modeled changes are negatively correlated (-0.27). Since the Asia-Pacific (APEC) domain in this study includes large areas in the maritime continents and DTR especially depends on the local land surface effects, it may be difficult for models to fully simulate DTR from daily temperature variations in the region of interest. Significant uncertainties in global models and the lack of ability to simulate DTR have been subjects of studies by Braganza et al. (2004), Stone and Weaver (2002) and Zhou et al. (2010). In particular, Zhou et al. (2010) stated that the much larger observed decrease in DTR suggests the possibility of additional regional effects of anthropogenic forcing that are usually unresolved in global climate models.

Temporal trends in temperature extremes in other sub-regions appear to be similar to those in the Asia-Pacific (APEC) region (not shown). Instead of showing all temporal trends in other sub-regions, correlation coefficients between observed- and model-based annual temperature extreme indices for the current climate period (1961-2000) are presented in Fig. 4. This figure can roughly explain the ability of the model to represent observed year-to-year variability of temperature extremes. For warm absolute-based indices (i.e., summer days (Fig. 4(a)) and tropical nights (Fig. 4(b)), South Asia (SAS) and Southeast Asia (SEA) show relatively higher correlations compared to other regions. This pattern might be related to the geographical features of the regions that are more consistent with the definition of the indices. The variability of observed trends in frost days is well captured by the models, especially in the Tibetan Plateau (TIB) and South Asia (SAS). Compared to absolute-based indices, percentile-based minimum temperature-related indices (Figs. 4(e) and (g)) exhibit higher correlations over broader regions, especially in the Tibetan Plateau (TIB), East Asia (EAS), South Asia (SAS), and Southeast Asia (SEA). This might imply that models can reasonably capture the variability of minimum temperature-related extremes in the sub-tropical and tropical regions. The higher correlations in minimum temperature-related indices are shown both in absolute-based indices (Figs. 4(b) and (d)) and percentile-based indices (Figs. 4(e) and (g)) compared to those in maximum temperature-related indices (Figs. 4(a) and

(c) and Figs. 4(f) and (h)). The variability of the warm spell duration index (WSDI) can be captured by models to some extent, especially in Northern Asia (NAS), Central Asia (CAS), and the Tibetan Plateau (TIB). This might suggest that models are likely to better simulate observed temporal trends in warm spell duration, especially in drier regions.

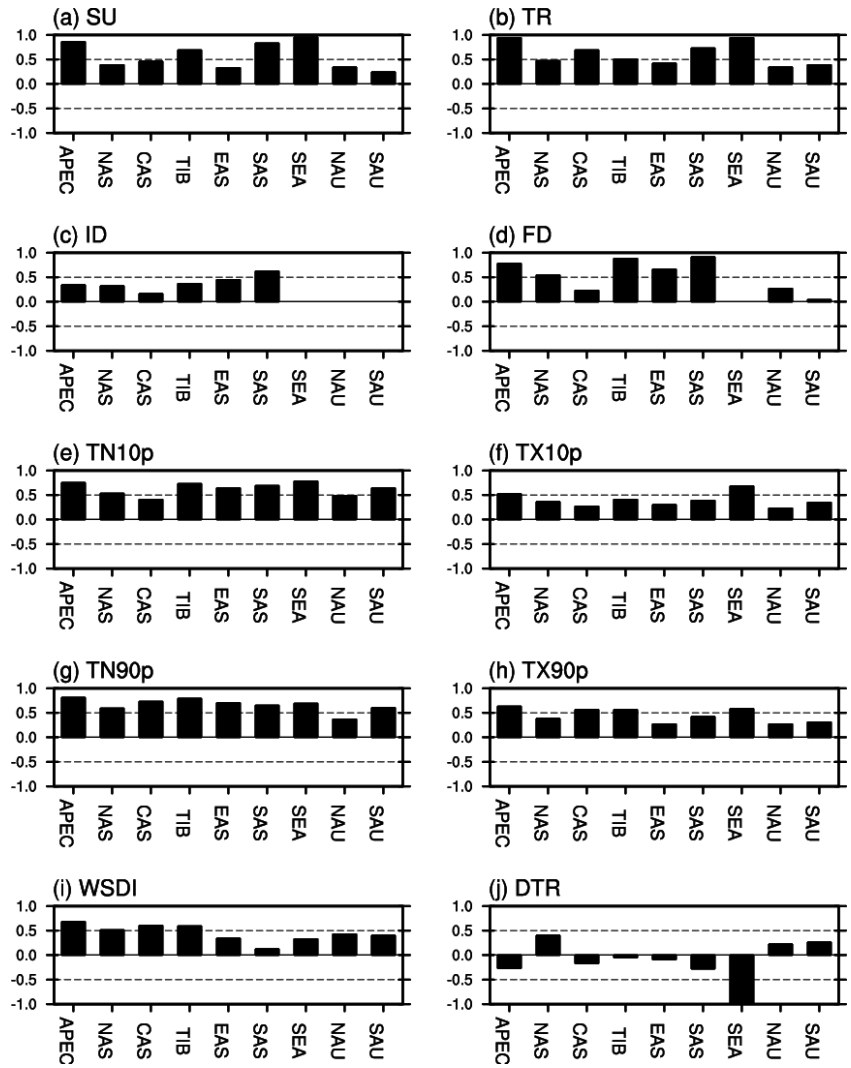

Figure 4 Correlation coefficients between observed- and model-based annual temperature extreme indices for the current climate period (1961-2000). Region classification and areas of each region are shown in Fig. 1.

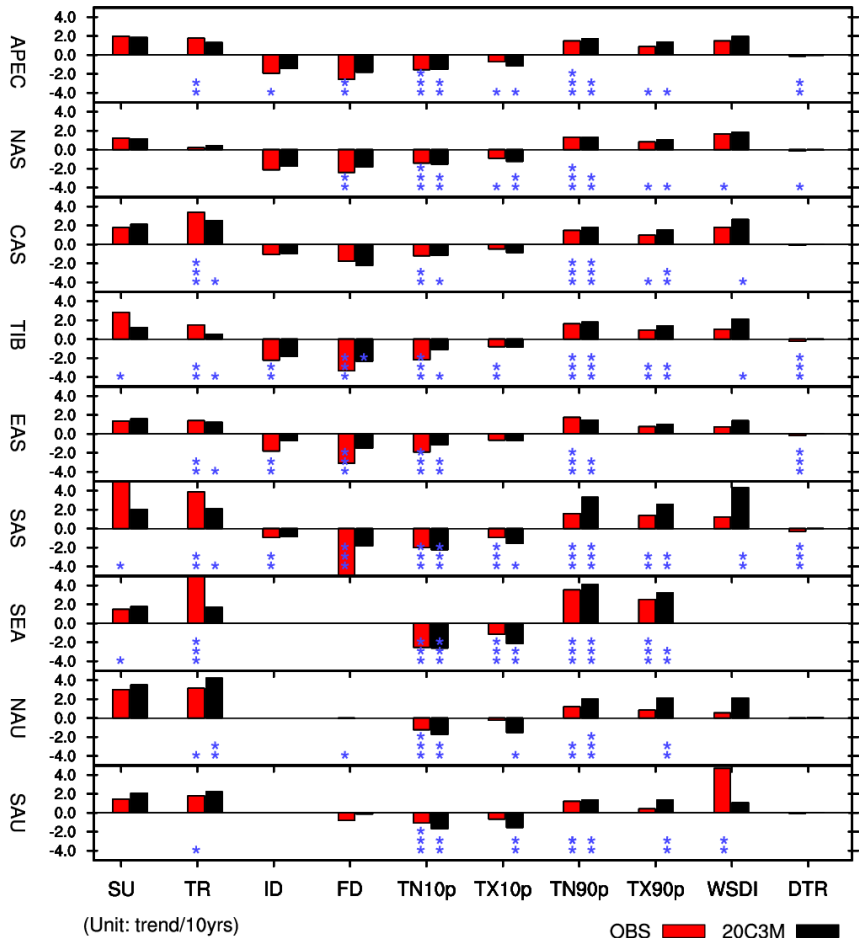

Figure 5 Decadal OLS trends and Mann-Kendall significance test of long-term (40 years, 1961-2000) annual indices of temperature in the present climate. OBS (red) indicates observations and 20C3M (black) gives the averages for four model simulations. Statistics from the Mann-Kendall significance test are also denoted by asterisks: significant at 0.1 (*), 0.05 (**), and 0.01 (***) levels, respectively. Region classification and the area of each region are shown in Fig. 1.

The general reliability and deficiency of global models in capturing the trends in temperature extremes are well shown in Fig. 5, in which area-averaged trends and their statistics for a significance test over each region are given. As shown in time series (Fig. 3) and with correlation coefficients (Fig. 4), the signs of simulated warming trends in all indices are in good agreement with those of observed warming trends with the exception of the Diurnal temperature range (DTR).

Both model simulations and observations show that the number of summer days (SU) increased by 2 days per decade in the Asia-Pacific (APEC) region. In the Tibetan Plateau (TIB, 3 days), South Asia (SAS, 5 days), and Northern Australia (NAU, 3 days), the number of summer days increased more than the averages over the Asia-Pacific (APEC) region. Models simulate an increase in the number of summer days in those regions, which is similar to or less than the observed increasing trends. In the Asia-Pacific (APEC) region, the number of tropical nights (TR) shows an increasing trend (2 days per decade) similar to that of the number of summer days. Observations show that the number of tropical nights increased more in tropical regions such as South Asia (SAS, 4 days), Southeast Asia (SEA, 11 days), and Northern Australia (NAU, 3 days) than in other regions. The models simulate fewer changes in the number of tropical nights. The numbers of icing days (ID) and frost days (FD) tend to decrease both in model simulations and observations. In the Tibetan Plateau (TIB), East Asia (EAS), and South Asia (SAS), the observed number of icing days and frost days (ranging from 3~7 days) decreased more than in other regions. The models simulate fewer changes in those extremes.

With a focus on the percentile-based indices, two things are clear. Firstly, the indices of temperature extremes indicate comparable warming between cool tails (-1.5 %, TN10p and -0.7 %, TX10p) and warm tails (1.7 %, TN90p and 0.9 %, TX90p) of the distributions of daily minimum and maximum temperature in the Asia-Pacific (APEC) region. Comparable warming between the two tails is shown both in observations and in model simulations over all regions. This result indicates shifted temperature distributions with no changes in parameters (e.g., scale) other than in the mean in the reference period; that is, simulated temperature variance remains unchanged from the current climate. Secondly, the observational changes in nighttime indices (-1.5 %, TN10p and 1.7 %, TN90p) appear larger than those in daytime indices (-0.7 %, TX10p and 0.9 %, TX90p), thus decreasing changes in diurnal temperature range (DTR, -0.14) are observed in the Asia-Pacific (APEC) region. However, global models produce similar trend magnitudes between nighttime indices (-1.50 %, TN10p and 1.71 %, TN90p) and daytime indices (-1.17 %, TX10p and 1.34 %, TX90p) in the region. In other words, global models seem to produce the same trend magnitudes in daytime and nighttime warming in response to the observed

forcing. Again, the difficulty global models have in simulating diurnal temperature range (DTR) has been examined by many studies, and the differences between the nighttime and daytime warming trends are shown also in other regions. However, both the model simulations and observations show the changes represented in the percentile-based temperature extremes tend to be larger in Southeast Asia (SEA) than in many other regions. Observations show that the warm spell duration index (WSDI) increased as much in Southern Australia (SAU) as in other regions, but the greatest increase is simulated in South Asia (SAS).

3.1.2 Precipitation extremes

Global models show more uncertainty in simulating changes in precipitation extremes than in temperature extremes (Fig. 6). Based on the spatial trends in precipitation extremes shown in Fig. 6, the models perform poorly in capturing temporal variability in the extremes in many regions. Comparison of changes in observations with those in model simulations does not show distinct agreement. The spatial trends in indices for precipitation extremes over the Asia-Pacific (APEC) region reflect spatially mixed and complex features in precipitation extremes. In addition, there are insignificant observed and simulated trends in precipitation indices over the Asia-Pacific (APEC) region during the reference period. This is in good agreement with the findings of Choi et al. (2009). They found no systematic and regional trends in total precipitation, or in the frequency and duration of extreme precipitation events, over the period of 1955-2007.

Time series for each of the precipitation indices calculated from both observations and model simulations indicate that models underestimate observed monthly maximum 1-day precipitation (RX1day) and precipitation intensity (SDII) in the Asia-Pacific (APEC) region (Fig. 7). Model simulations also tend to underestimate the number of heavy precipitation days (R10mm) and annual total precipitation (PRCPTOT, R95pTOT and R99pTOT). Model simulations tend to well represent observed changes in consecutive dry days (CDD), but they tend to overestimate observed changes in consecutive wet days. Temporal changes in precipitation extremes imply that models tend to produce insufficient daily rainfall amounts and inadequately

capture day-to-day rainfall variation. However, this may be expected in examining the ability of climate models. Given that precipitation has greater variability in space and time than temperature, and because precipitation extremes would be affected by individual storm events or convections, models are expected to be less skillful at simulating patterns of precipitation extremes than temperature extremes (Alexander and Arblaster, 2009). This is a main reason why the coarse resolution global models have limitations in simulating precipitation extremes. It is also notable that all observation-based indices (HadEX) are first calculated for each observation point and then interpolated onto the latitude-longitude rectangular grid, while all the model-based indices are calculated from the variables representative of a grid box. These computational differences may cause systematic disparities in the probability distributions of spatially inhomogeneous data such as precipitation (Sillman and Roeckner, 2008). Therefore, this discrepancy should be considered when comparing observation-based and model-based indices for precipitation extremes.

Fig. 8 presents correlation coefficients between observation- and model-based annual temperature extreme indices for the current climate period (1961-2000) in each region. Model simulations tend to fail to capture extreme precipitation amount and intensity, especially in South Asia (SAS) and Southeast Asia (SEA). The inability of the models to capture extreme precipitation in South Asia (SAS) is likely linked to the coarse resolution of models, as the heavy rainfall over this region tends to be highly localized and associated with orographically induced rainfall (IPCC, 2007a). Wang et al. (2004) also found the ability of global models to simulate observed interannual rainfall variations to be poorest in Southeast Asia (SEA). Since current AOGCMs continue to have some significant shortcomings in representing ENSO variability, the difficulty of projecting changes in ENSO-related rainfall in this region is compounded (IPCC, 2007a). The inability of the models to simulate precipitation variations would be reflected in simulations of changes in precipitation extremes. Fig. 9 shows area-averaged trends for each of the precipitation extreme indices and their statistics for a significance test for each region. There is no evidence of clear trends in monthly maximum 1-day precipitation amount (RX1day), precipitation intensity (SDII), the number of heavy precipitation days (R10mm), consecutive dry days (CDD), and consecutive wet days (CWD). Meanwhile, observations show

increasing trends in annual total precipitation wet days (PRCPTOT), very wet days (R95pTOT), and extremely wet days (R99pTOT), especially in Northern Asia (NAS), South Asia (SAS), Northern Australia (NAU), and Southern Australia (SAU), but they show decreasing trends in Southeast Asia (SEA). Model simulations are very unlikely to capture the trends in those precipitation extremes over all regions.

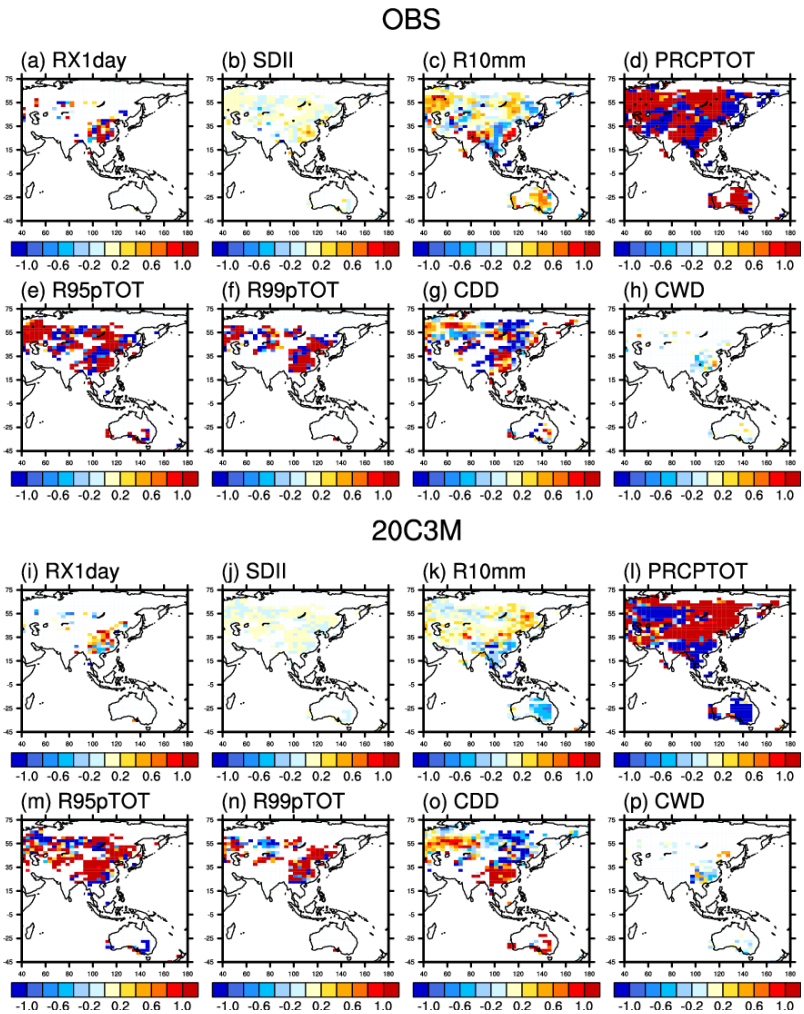

Figure 6 Observed (upper two panels, OBS) and simulated (lower two panels, 20C3M – averages for four model simulations) decadal spatial trends in precipitation extremes calculated between 1961 and 2000 over the Asia-Pacific (APEC) region. Model data are masked out with grid boxes which have observations. Stippling indicates the trend is significant at the 0.05 level.

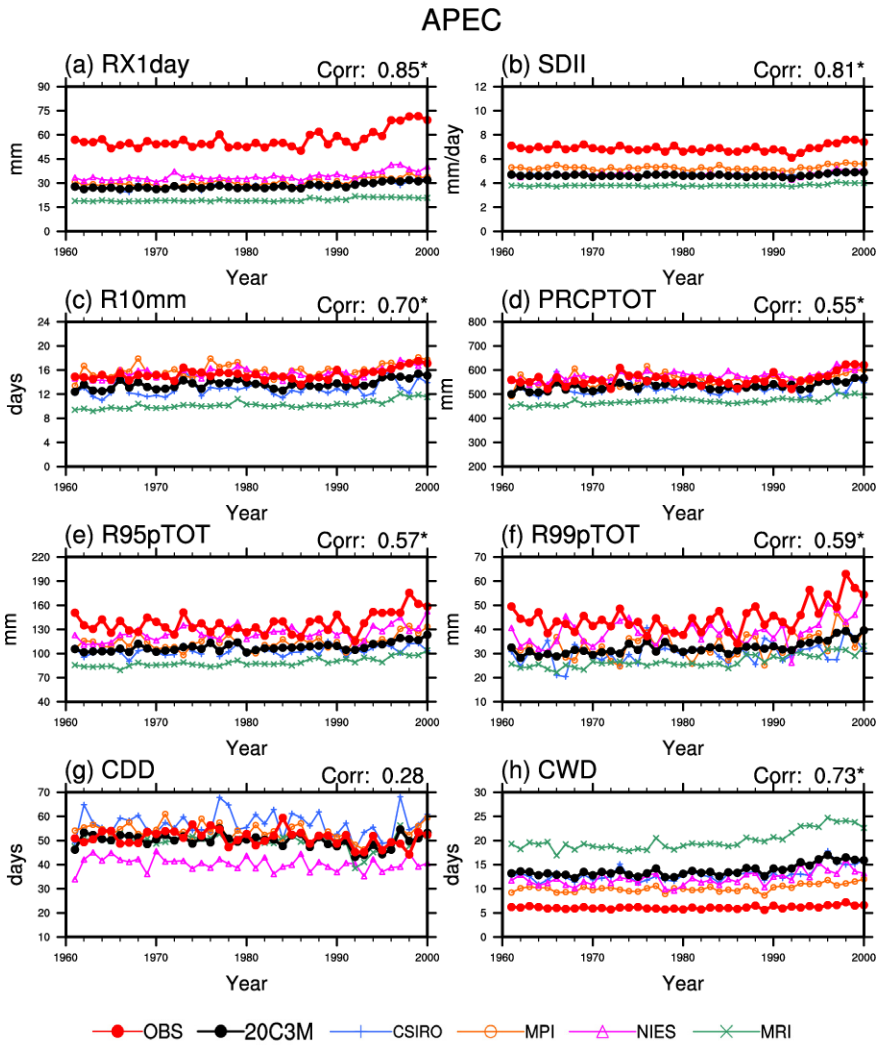

Figure 7 Temporal trends in precipitation extremes: the indices for precipitation extremes are averaged over the Asia-Pacific (APEC) region for the period of current climate (1961-2000). The black and red thick lines indicate the model simulations (20C3M – averages for four model simulations) and the observation (OBS), respectively. The thin colored lines with small symbols indicate each model simulation. Correlations between 20C3M and OBS and their significant tests (asterisk: significant at the 0.05 significance level) are also given.

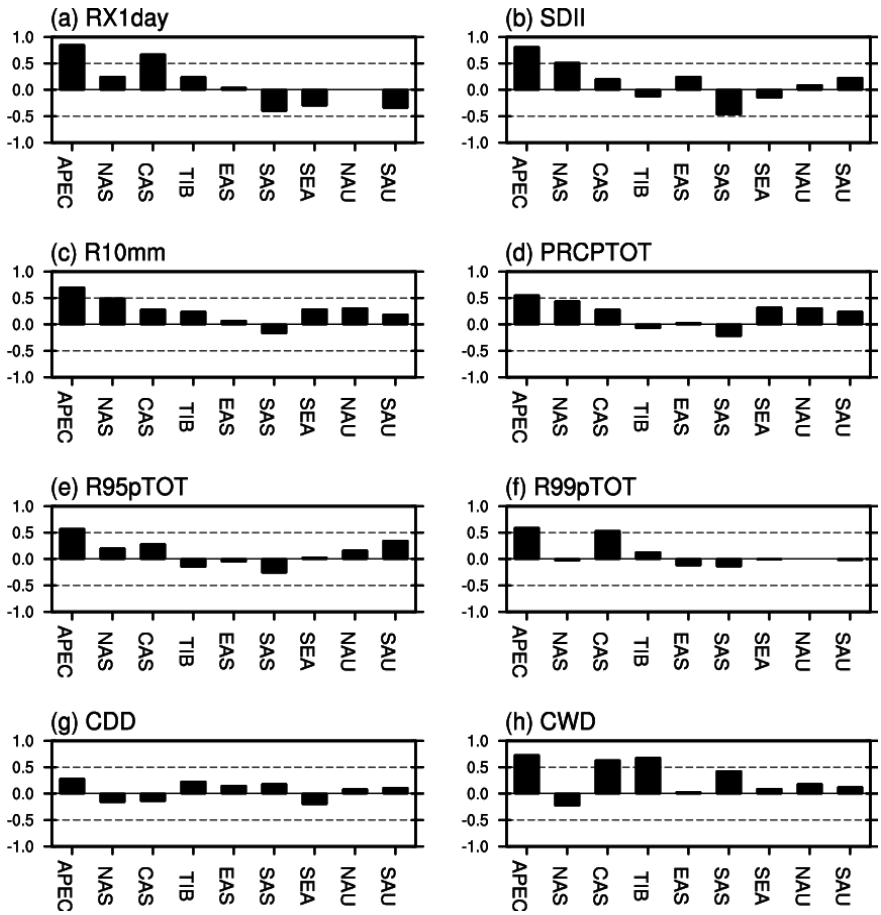

Figure 8 Correlation coefficients between observed- and model-based annual precipitation extreme indices for the current climate period (1961-2000). Region classification and areas of each region are shown in Fig. 1.

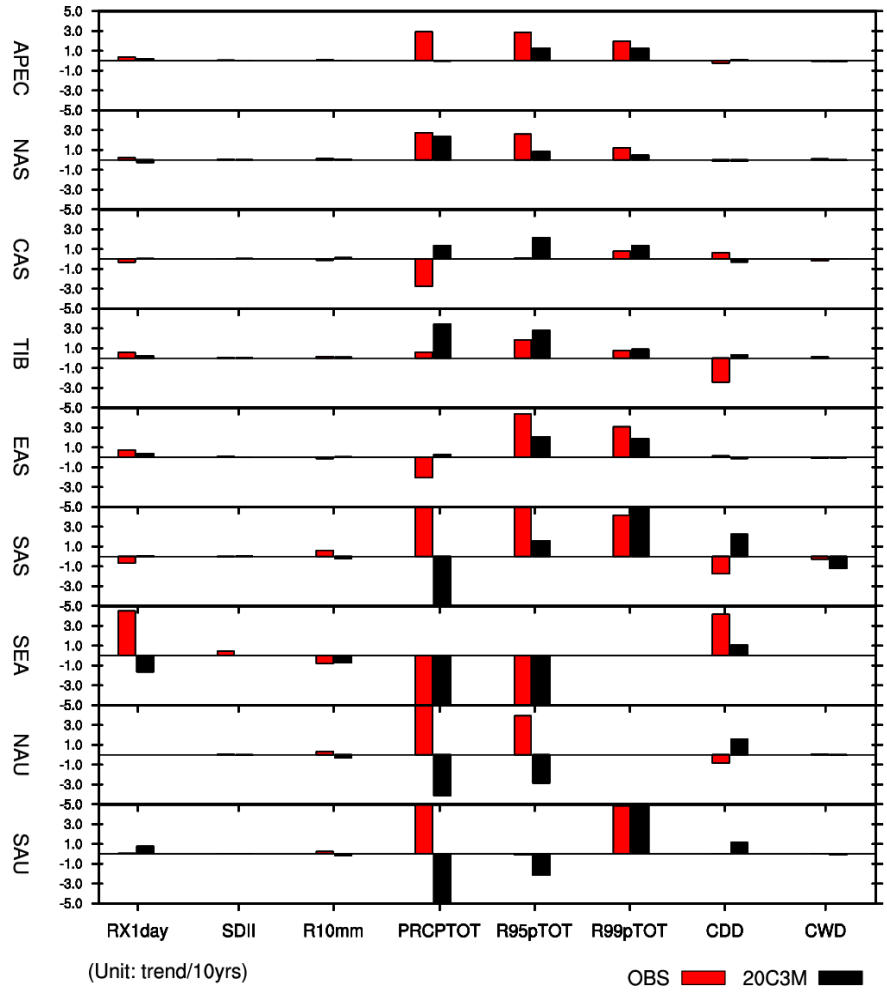

Figure 9 Decadal OLS trends and Mann-Kendall significance test of long-term (40 years, 1961-2000) annual indices of precipitation in the present climate. OBS (red) indicates observations and 20C3M (black) gives the averages for four model simulations. Statistics from the Mann-Kendall significance test are also denoted by asterisks: significant at 0.1 (*), 0.05 (**), and 0.01 (***) levels, respectively. Region classification and the areas of each region are shown in Fig. 1.

Based on the comparison between observational and modeled precipitation extremes for the past several decades, it can be concluded that the reliability of simulated daily extreme precipitation data from current global models is low even for the past climate. Though precipitation does not show good agreement with observations during the reference climate period, several studies suggested that the

changes between future and reference simulations tend to be insensitive to the characteristics of the baseline climate when viewed as anomalies with respect to their respective reference climates. This result is partly due to the cancellation of systematic errors in the underlying model that occurs when taking the difference between future and reference climates (Hagemann and Jacob, 2007; Sushama et al., 2006). Therefore, if we could produce similar change patterns of precipitation extremes in the future climate using several different model projections, the result would be considered robust and valuable.

3.2 Projected future changes in extremes over the Asia-Pacific region

3.2.1 Temperature extremes

For projected future changes in extremes from multiple climate change scenarios (A1B, A2 and B1), the changes from 1981 to 2000 are taken to characterize the current climate condition (20C3M) and are compared with those from 2081 to 2100, which are taken to represent the projected future climate (SRES). To see the projected future changes in extremes, the ensemble mean projected changes in extremes are simply defined as the differences between the averages for the future and current climates. Fig. 10 displays the ensemble mean projected changes in temperature extremes between the A1B and 20C3M scenarios. Spatial patterns of changes in temperature extremes are shown only for the A1B experiment, which is based on the intermediate level of greenhouse gas emission. However, similar patterns are found for the other scenarios. From the spatial distribution of projected changes in temperature extremes, warmer conditions are projected for the future climate over all of the considered regions except the Tibetan Plateau (TIB). From Figs. 10(a)-(d), it is shown that in the Tibetan Plateau (TIB), lower temperature extremes such as frost days (FD) and icing days (ID) are expected to significantly decrease, whereas higher temperature extremes such as summer days (SU) and tropical nights (TR) are expected to increase in the late 21st century. This again may be due to the models' uncertainty (e.g., temperature underestimation) in resolving geographical effects in the high and topographically complex regions and/or the threshold used

to define those indices (25°C for SU and 20°C for TR).

From thinner lower tails (Figs. 10(e)-(f)) and thicker upper tails (Figs. 10(g)-(h)) of temperature extremes, it is expected that the likelihood of more intense warm extreme events will tend to increase in the future climate. It is also shown that warm extremes are expected to increase much faster than cool extremes, and the asymmetric warming seems to be consistent across the terrestrial areas of the Asia-Pacific (APEC) region. In particular, it is notable that the changes in the upper tails of temperature extremes (i.e., toward warm extremes) are expected to be significantly large in South Asia (SAS), Southeast Asia (SEA), and Northern Australia (NAU), perhaps implying that tropical regions (i.e., SAS, SEA, and NAU) in the Asia-Pacific (APEC) are expected to experience intensified warm extremes in the future in response to the specified forcing.

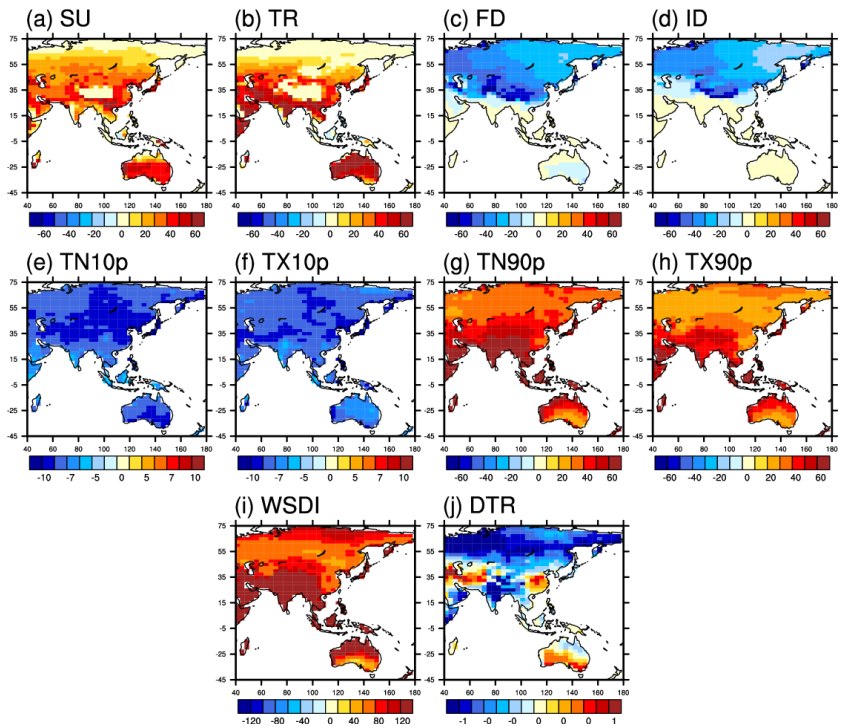

Figure 10 Projected changes in indices for temperature extremes in the Asia-Pacific (APEC) region. The changes are defined as differences between averages for four model simulations from A1B (2081-2100) and 20C3M (1981-2000) at each terrestrial grid point.

Fig. 10(i) reveals that the intensity of heat stress during hot periods is also expected to increase under projected future climate conditions in the Asia-Pacific (APEC) region. The increasing trends in heat stress are also expected to be large in South Asia (SAS), Southeast Asia (SEA), and Northern Australia (NAU). Based on the changes in warming extremes (Figs. 10(g)-(h)), those regions are expected to experience more frequent and long-lasting warm spells. Unlike other temperature extremes, changes in the diurnal temperature range (DTR) are not expected to be uniform across all regions. Decreasing changes in the diurnal temperature range (DTR) are expected to have a regional maximum in Northern Asia (NAU) and South Asia (SAS). The diurnal temperature range (DTR) is also expected to increase under the future climate scenario in Central Asia (CAS), the western inland area of East Asia (EAS) and Southern Australia (SAU),.

According to the IPCC (2007a), warming from annual mean temperature changes (change between 1980 to 1999 and 2080 to 2099, averaged over 21 multi-model dataset) over Asia tends to be larger from sea to land (South Asia, SAS), in the northern inland area (East Asia, EAS), and in the interior of those landmasses, than over the surrounding coastal regions (Southeast Asia, SEA), high-altitude areas (Central Asia (CAS) and the Tibetan Plateau (TIB)). However, it is found in this study that warming of extreme temperature changes is expected to differ from the mean temperature changes. Fig. 11 presents area-averaged projected changes in indices for temperature extremes in each region. Summer days (SU) and Tropical nights (TR) are expected to increase more in Central Asia (CAS), East Asia (EAS), and Northern Australia (NAU). Icing days (ID) and frost days (FD) are expected to decrease more in Northern Asia (NAS) and the Tibetan Plateau (TIB).

Decreasing changes in cool extremes calculated from the lower tail thickness of the temperature distribution (i.e., TN10p and TX10p) are expected to be relatively large in the northern landmass areas such as Northern Asia (NAS), Central Asia (CAS), the Tibetan Plateau (TIB), and East Asia (EAS). However, increasing changes in warm extremes represented from the upper tail thickness of the temperature distribution (i.e., TN90p and TX90p) are expected to be comparatively large in the tropical inland areas such as South Asia (SAS) and Southeast Asia (SEA). That is, decreasing changes in cool extremes are expected to be large in subtropical areas, whereas increasing

trends in warm extremes are expected to be large in tropical areas of the Asia-Pacific (APEC) region. As shown in Fig. 10(i), increasing trends in warm spell duration are expected to be larger in tropical areas such as South Asia (SAS) and Southeast Asia (SEA) than in other regions.

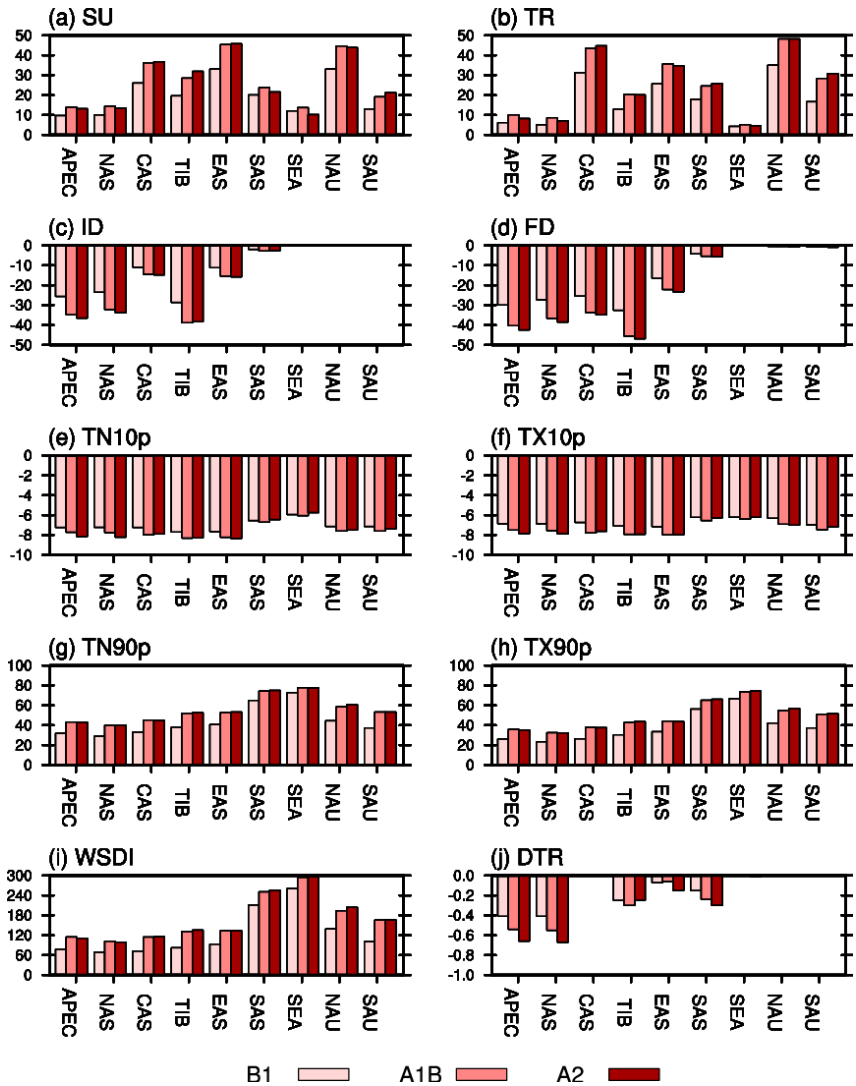

Figure 11 Area-averaged projected changes in indices for temperature extremes in each region. The changes are defined as the differences between the averages of four model simulations from A1B (2081-2100) and 20C3M (1981-2000) at each terrestrial grid point. Region classification and the areas of each region are shown in Fig. 1.

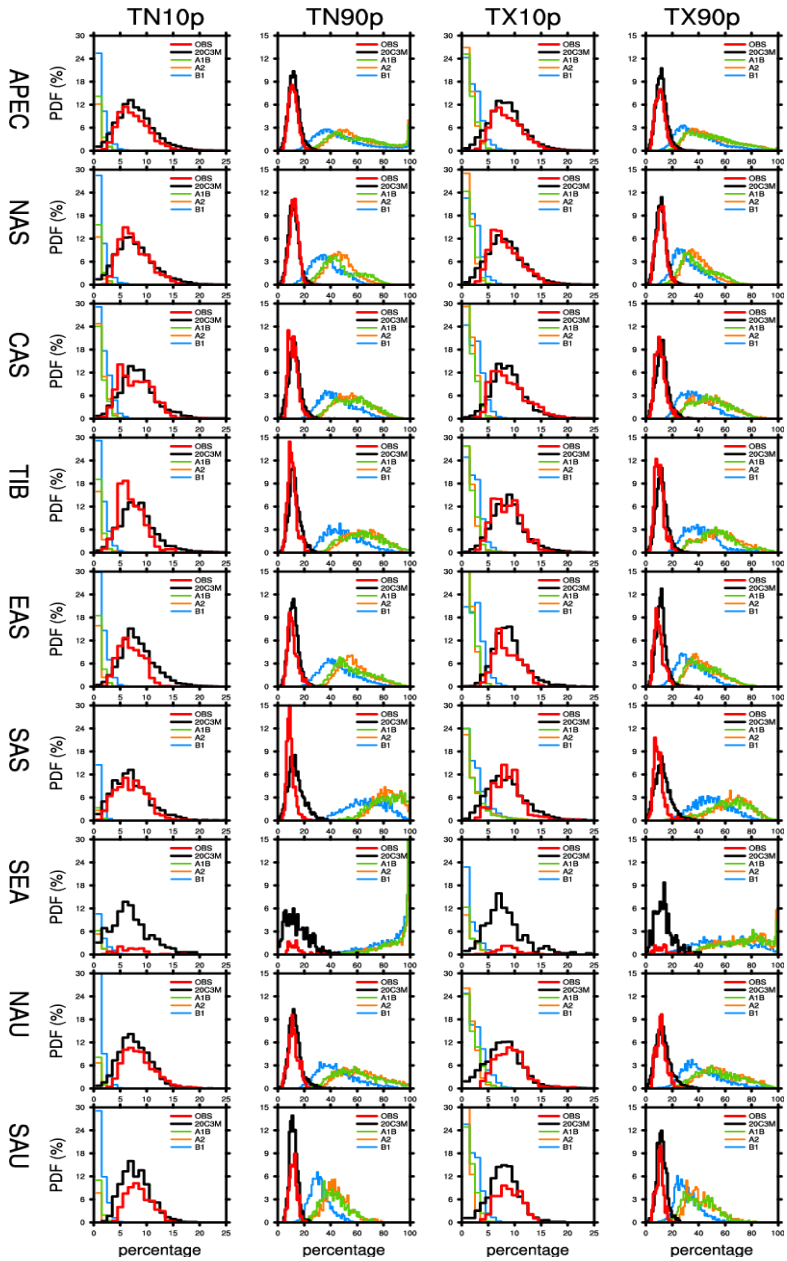

Figure 12 PDFs of the annual frequency of extreme temperature from observations (OBS) and averages for four model simulations under the current climate (20C3M) and future climate (A2, A1B and B1) for grid points over terrestrial region for two 20-year periods: (1) 1981-2000 (OBS and 20C3M) and (2) 2081-2100 (A2, A1B and B1). The X-axis means the percentage of days when Tmin (first two columns) or Tmax (last two columns) is greater and/or less than 10th (1st and 3rd column) and/or 90th (2nd and 4th column) percentile.

It is also clear from Fig. 11 that projected changes in temperature extremes depend on the level of emission forcing in the three different scenarios; that is, the higher the level of greenhouse gases, the higher is the frequency of temperature extremes. This is in agreement with the findings of previous studies. For example, Tebaldi et al. (2006) and Alexander et al. (2009) showed that differences in the relative magnitude of trends vary according to different emissions scenarios.

Probability distribution functions (PDFs) of several indicators are also considered. The indicators include cool and warm nights (TN10p and TN90p) and cool and warm days (TX10p and TX90p) for temperature extremes and are explained in Table 1. PDFs are calculated using the value of indices at land grid points over each area in the Asia-Pacific (APEC) region for two 20-year periods including 20C3M (1981-2000) and three SRES experiments (2081-2100). A comparison of PDFs of temperature extremes from observations and current climate simulations (Fig. 12) indicates that an ensemble of global climate models tends to show reliable predictability for temperature extremes except for Southeast Asia (SEA). Models tend to simulate much stronger temperature extremes than are shown in observations in Southeast Asia (SEA); however, models tend to reasonably well simulate the median and variance of the probability distribution of temperature extremes in other regions. Since Fig. 12 represents the probability distribution of the lower and upper tail distributions (i.e., extremes) of temperature, the agreement between the models and observations in these PDFs suggests that global models tend to produce reasonable characteristics of annual temperature extremes as a response to observed forcing agents. Therefore, we can have some degree of confidence in analyzing projected temperature extremes in response to certain forcing scenarios.

Regarding the projected temperature extremes shown in Fig. 12, comparisons of ensemble mean PDFs between current and future climate conditions suggest that in the late 21st century, the median of the frequency of extreme temperature is systematically shifted to warmer extremes for higher extreme events and to the colder extremes for lower extreme events. It is also interesting to note that the annual number of warm extremes, such as TX90p and TN90p, is expected to increase much faster than expected due to the corresponding decrease in the number of cool

extremes, such as TX10p and TN10p, at the end of 21st century. This asymmetrical warming indicates that the chance of occurrence of intense temperature extremes is expected to shift to warm extremes in future climate conditions. This tendency toward asymmetrical warming is expected over all regions in the Asia-Pacific (APEC) region. It is also notable that the median and variance of projected cool extremes (i.e., TN10p and TX10p) are expected to be similar among all areas; however, those of projected warm extremes (i.e., TN90p and TX90p) are expected to be much more geographically dependent. In particular, the median of warm extremes (TN90p and TX90p) is expected to be larger in South Asia (SAS) and Southeast Asia (SEA) than in other regions. The variance of warm extremes is expected to be large in the Tibetan Plateau (TIB), South Asia (SAS), Southeast Asia (SEA), and Northern Australia (NAU).

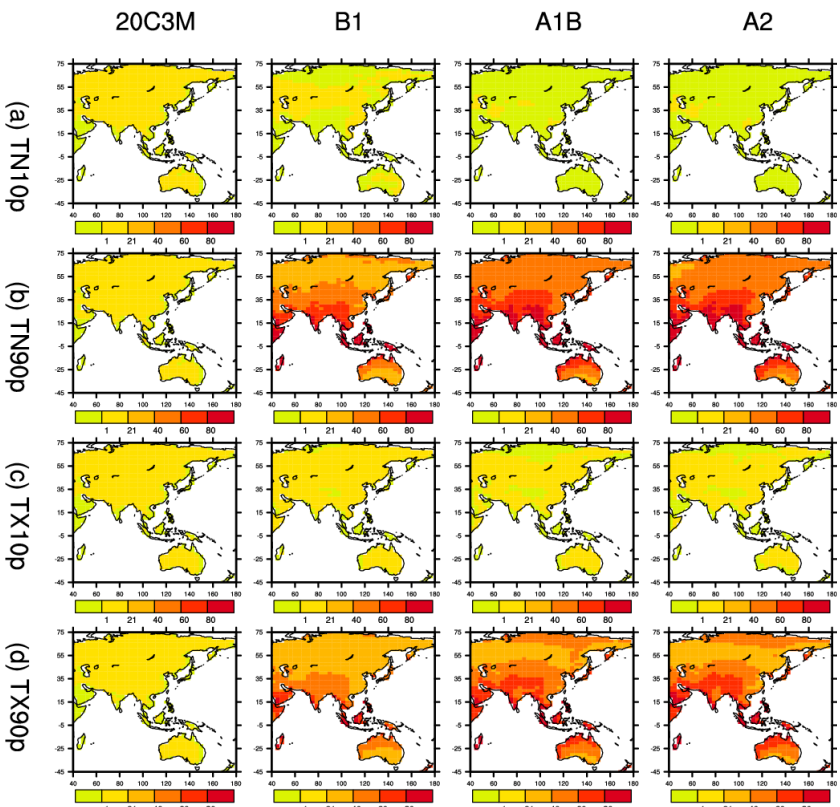

Figure 13 Spatial distribution of the model ensemble average of percentile-based indices calculated from four global models used in this study for two periods: 20C3M (1981-2000) and B1, A1B, and A2 (2081-2100).

With respect to this issue, the spatial distributions of model ensemble averages (Fig. 13) and standard deviations (Fig. 14) of percentile-based temperature indices are calculated from four global models for the current and future climates: 20C3M (1981-2000) and A2, A1B and B1 (2081-2000). From the spatial distribution of model ensemble averages (Fig. 13), it is shown that warm events (TN90p and TX90p) are expected to increase more than cool events (TN10p and TX10p). More, the increasing tendency towards warm extremes (TN90p and TX90p) is expected to be largest in tropical regions such as South Asia (SAS), Indochina, Southeast Asia (SEA), and Northern Australia (NAU). This distribution of warming change might imply that tropical regions make a considerable contribution to the large median of projected warm events (PDFs in Fig. 12) than do other regions in higher latitudes.

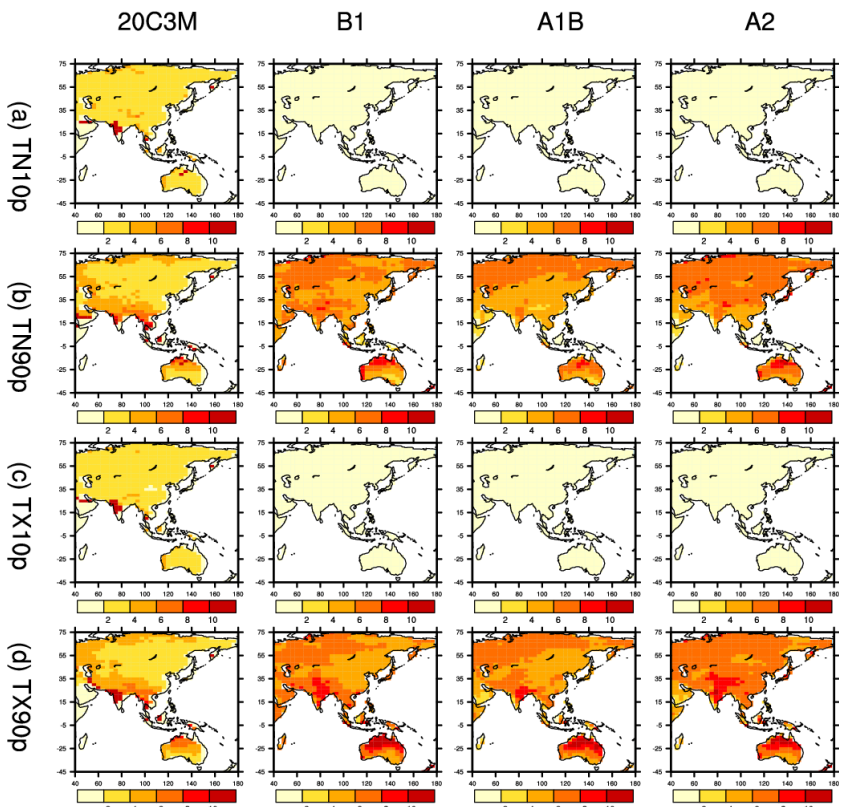

Figure 14 Spatial distribution of model ensemble standard deviations of percentile-based indices calculated from the four global models used in this study for two periods: 20C3M (1981-2000) and B1, A1B, and A2 (2081-2100).

From the spatial distribution of model standard deviations (Fig. 14), it is shown that interannual variability is expected to be larger for warm events (TN90p and TX90p) than for cool events (TN10p and TX10p), which implies an increase in temperature extreme variability for warm events. In addition, the standard deviation of warm events is expected to be larger in South Asia (SAS) and Northern Australia (NAU) than in other regions. The tendency towards large interannual variability of warm events over these regions in the current climate (20C3M) is expected to be intensified in the future warmer climate. Therefore, large variance of warm events in the PDFs (Fig. 12) in the future climate might be attributable to an increase in temperature extreme variability, especially in South Asia (SAS) and Northern Australia (NAU). From Figs. 13-14, it may be concluded that asymmetric warming is projected to occur in the 21st century. In particular, tropical regions (South Asia (SAS), Indochina, Southeast Asia (SEA), and Northern Australia (NAU)) may be expected to be influenced by consistent and more intense warm extremes, and South Asia (SAS) and Northern Australia (NAU) may be expected to experience increased variability of temperature extremes in the late 21st century under the forcing scenarios.

As cold and warm extremes are associated with specific atmospheric circulation patterns in the Asia-Pacific (APEC) region, changes in airflow may be driving forces for the extremes. Cool extremes in winter are often associated with airflow from the snow-covered continent and in summer with airflow from the Pacific Ocean. It is reasonable to assume that cool extremes are less sensitive to large-scale warming than warm extremes, because of the latent heat of snow and thermal inertia of water (Klein Thank and Konnen, 2003). A systematic study of the relationship between changes in circulation and in cold and warm extremes is needed for a better understanding of the causes of the asymmetry in temperature extreme change, although this is beyond the scope of this study.

3.2.2 Precipitation extremes

IPCC (2007a) says that multi-model datasets indicate an increase in annual mean precipitation over most of Asia in the late 21st century, with the percentage increase being largest and most consistent among models in Northern Asia (NAS) and East

Asia (EAS). The main exception is Central Asia (CAS), where most models simulate decreases in mean precipitation. The spatial distribution of projected changes in precipitation extremes in this study is to some extent similar to the aforementioned changes in mean precipitation (Fig. 15). The patterns of changes in precipitation extremes appear similar among three different emission scenarios (not shown). Compared to the changes in temperature extremes, the projected changes in precipitation extremes appear spatially non-uniform across the region, but many economies located in South Asia (SAS), East Asia (SEA), Southeast Asia (SEA) and Northern Asia (NAS) are expected to undergo heavy precipitation extremes in the future climate. The amount of maximum 1-day precipitation (RX1day) and precipitation intensity (SDII) are expected to be large in South Asia (SAS) and East Asia (EAS). The amount of annual total precipitation in wet days (PRCPTOT) is expected to increase over most areas with the exception of Central Asia (CAS), and Northern (NAU) and Southern Australia (SAU). The fraction of annual high precipitation amounts due to very wet days (R95pTOT, Fig. 15(e)) and extremely wet days (R99pTOT, Fig. 15(f)) is expected to increase substantially over tropical (i.e. South East Asia (SEA)) and sub-tropical regions (i.e., South Asia (SAS) and East Asia (EAS)) under the projected climate change scenario. Thus, the likelihood of occurrence of flooding is expected to significantly increase in tropical regions and sub-tropical regions over the Asia-Pacific (APEC) region. The magnitude of changes in consecutive dry days (CDD, Fig. 15(g)) is expected to be larger than that in consecutive wet days (CWD, Fig. 15(h)) in the future climate. In particular, consecutive dry days (CDD) are expected to increase in Central Asia (CAS) and Northern (NAU) and Southern Australia (SAU). An increase of consecutive dry days (CDD) in Northern (NAU) and Southern Australia (SAU) is related to a decrease in the annual total precipitation amount (PRCPTOT). The eastern part of Northern Asia (NAU) and East Asia (EAS) are expected to experience a decrease in consecutive dry days (CDD).

Fig. 16 displays the area-averaged projected changes in indices for precipitation extremes in each region. Monthly maximum 1-day precipitation (RX1day) and precipitation intensity (SDII) are expected to increase over all regions; in particular, they are expected to increase most in East Asia (EAS), South Asia (SAS), and Southeast Asia (SEA). Extreme rainfall intensity (e.g., RX1day) and extreme rainfall amount

(SDII) are expected to increase in all regions, whereas the number of heavy rainfall days is expected to decrease in Southeast Asia (SEA) and Northern Australia (NAU). The amounts of annual total precipitation in wet days (PRCPTOT), very wet days (R95pTOT), and extremely wet days (R99pTOT) are expected to increase especially in East Asia (EAS), South Asia (SAS) and Southeast Asia (SEA), and to decrease or be unchanged in Northern (NAU) and Southern (SAU) Australia. Consecutive dry days (CDD) are expected to increase especially in Northern (NAU) and Southern (SAU) Australia, and to be almost unchanged in other regions. In addition, consecutive wet days (CWD) are expected to slightly decrease in Southeast Asia (SEA) and Southern Australia (SAU), although to a minimal extent.

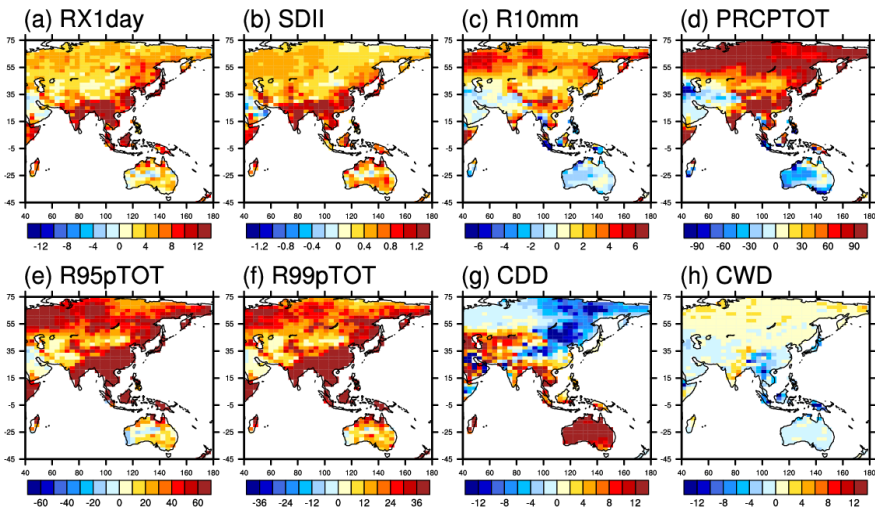

Figure 15 Projected changes in indices of precipitation extremes in the Asia-Pacific (APEC) region. The changes are defined as differences between averages for four model simulations from A1B (2081-2100) and 20C3M (1981-2000) at each terrestrial grid point.

Considering that there are differences in the relative magnitude of trends under various emission scenarios (Alexander et al., 2009; Tebaldi et al., 2006), the differences in the relative magnitude of trends in precipitation extremes under various emission scenarios are also considered. However, the differences in the precipitation extreme responses among the different scenarios are not as distinct as are those of the temperature extremes.

Fig. 17 presents the PDFs of the annual frequency of extreme precipitation. From the PDFs, it is shown that models are likely to underestimate observed extreme precipitation amounts over all regions. In addition, the projected median and variance of the PDFs of the frequency of extreme precipitation are not expected to change significantly. It is expected, however, that precipitation extremes will tend to have thicker and longer upper tails in the future climate compared to those in the current climate, implying that the intensity of heavy precipitation extremes will probably increase under the projected future warmer climate.

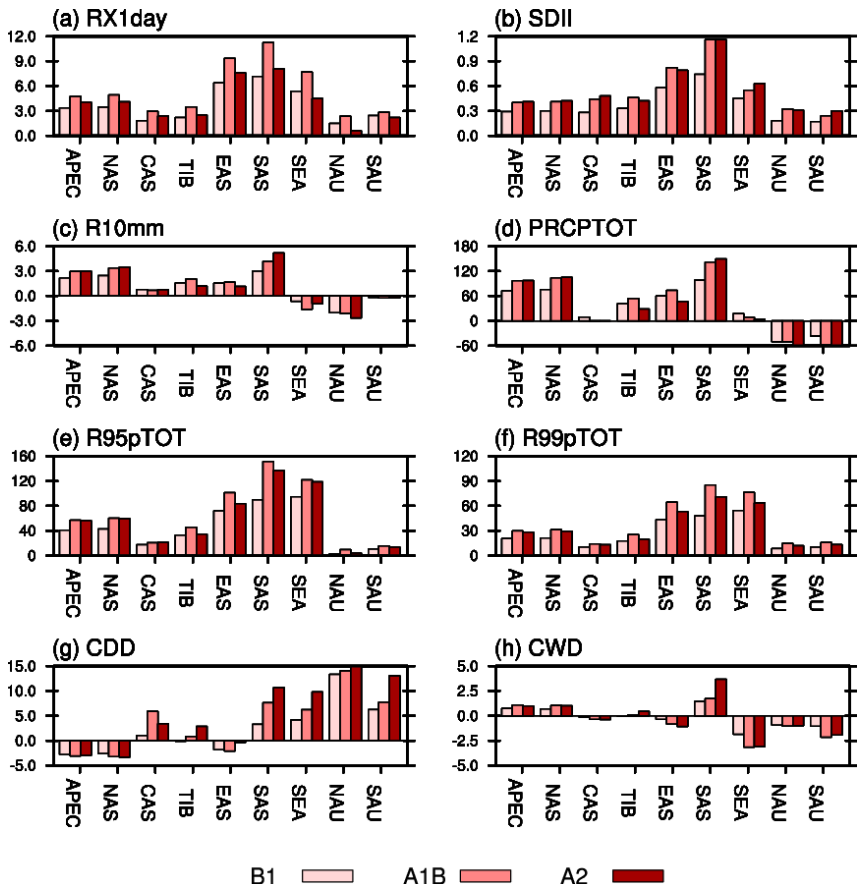

Figure 16 Area-averaged projected changes in indices for precipitation extremes in each region. The changes are defined as the differences between averages for the four model simulations from A1B (2081-2100) and 20C3M (1981-2000) at each terrestrial grid point. Region classification and the areas of each region are shown in Fig. 1.

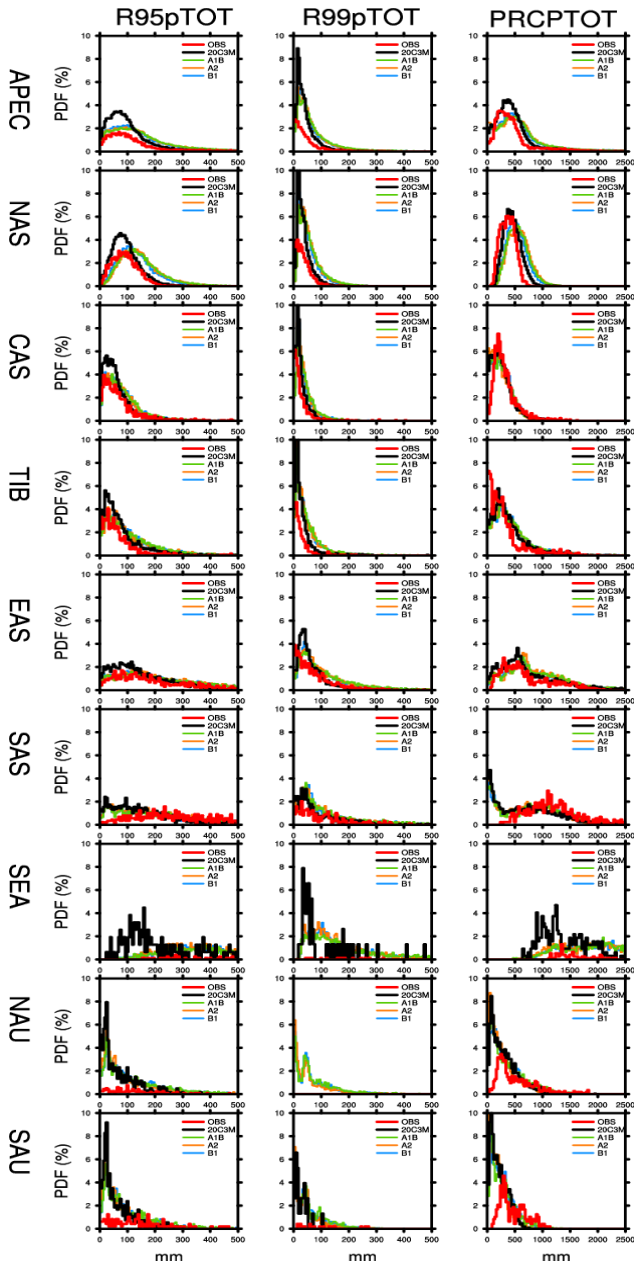

Figure 17 PDFs of the annual frequency of extreme precipitation from observations (OBS) and averages for four model simulations under the current climate (20C3M) and future climate (A2, A1B and B1) for grid points over terrestrial region for two 20-year periods: (1) 1981-2000 (OBS and 20C3M) and (2) 2081-2100 (A2, A1B and B1). The X-axis means the percentage of days when Tmin (first two columns) or Tmax (last two columns) is greater and/or less than 10th (1st and 3rd column) and/or 90th (2nd and 4th column) percentile.

4. SUMMARY AND CONCLUSION

As noted by Alexander and Arblaster (2009), Chen et al. (2010), Hegerl et al. (2004), Kiktev et al. (2003), Tebaldi et al. (2006), Tebaldi and Knutti (2007) and in many other studies, the projection of changes in climate extremes using global climate models is quite challenging, mainly due to the coarse resolution and the lack of finer parameterization of AOGCMs. Despite these limitations, it has been proven that global climate models can to some extent reliably simulate the mean values and variability of extreme precipitation and temperature events (Marengo et al., 2010; Rusticucci, 2010). Therefore, it is still important to evaluate the ability of global climate models to make general statements with respect to the spatial and temporal patterns of climate extremes in the region of interest. In the current study, analysis is done with foci on 1) comparison of spatial and temporal trends with model- and observation-based indices for extreme events in the present climate, and 2) investigation of projected future changes in extremes over the Asia-Pacific region. A set of climate extreme indices are simultaneously considered in this study, and the indices are based on absolute thresholds and/or percentile thresholds.

As a way of examining the ability of global climate models to simulate the trends in the current climate, the temporal and spatial trends evident in observations are compared with those estimated by global models. Observed temporal trends and spatial patterns in temperature extreme indices indicate apparent and significant warming that is to some extent in agreement with the simulated trends. Observations show large warming in extremes in high-topographic regions such as the eastern part of Northern Asia (NAS), the Tibetan Plateau (TIB), and East Asia (EAS), whereas models simulate weaker warming in those regions. Models are likely to simulate more warming in the sub-tropical regions such as South Asia (SAS), the western part of East Asia (EAS) and Northern Australia (NAU). The disparity between regions may be related to the models' inability to represent the effects of the dramatic topographic relief in certain regions and distorted albedo effects due to snow cover (IPCC, 2007a).

Observations show that the number of summer days increased more in the Tibetan

Plateau (TIB), South Asia (SAS), and Northern Australia (NAU) and the number of tropical nights increased more in the tropical regions (South Asia (SAS), Southeast Asia (SEA), and Northern Australia (NAU)). However, the mmodels tend to underestimate the amount of warming in those extremes. In observations, the number of icing days and frost days decreased more in the Tibetan Plateau (TIB), East Asia (EAS) and South Asia (SAS), whereas the models tend to simulate fewer changes in those extremes. Observations show the duration of warm spells to increase, especially in Southern Australia (SAU), and to decrease in the Yangtze River region. However, the models fail to simulate the changes in warm spell duration over those regions.

Compared to the changes in temperature extremes, the changes in precipitation extremes are not well represented by global models. There is no evidence for clear trends in monthly maximum 1-day precipitation amount, precipitation intensity, the number of heavy precipitation days. Observations show increasing trends in annual total precipitation in wet days, very wet days, and extremely wet days, especially in Northern Asia (NAS), South Asia (SAS), and Northern (NAU) and Southern Australia (SAU). However, model simulations are very unlikely to capture the trends in those precipitation extremes over all regions.

Warmer conditions are expected over all of the considered regions under the projected future climate with the exception of the Tibetan Plateau (TIB). In the Tibetan Plateau (TIB), cool extremes (frost days and icing days) are expected to significantly decrease, whereas warm extremes (summer days and tropical nights) are expected to show less change in the late 21st century. This again may be due to either model uncertainty (e.g., temperature underestimation) in resolving geographical effects in the high topographic regions or the threshold used to define those indices. It is also notable that the tendency toward warm extremes is expected to be greatest in South Asia (SAS), Southeast Asia (SEA), and Northern Australia (NAU), which are expected to experience more frequent and long-lasting warm spells.

Asymmetric extreme events are expected to arise in the late 21st century. It is interesting that the annual number of warm extreme events (TX90p and TN90p) is expected to increase more, with greater variance, than the number of cool extreme

events (TX10p and TN10p). This asymmetric warming indicates that frequency of occurrence of intense temperature extremes is expected to be greater for warm extremes than for cool extremes in the future climate. From model ensemble averages and standard deviations of percentile-based extreme indices, it is expected that tropical regions (South Asia (SAS), Indochina, Southeast Asia (SEA), and Northern Australia (NAU)) may make a greater contribution to the large median number of projected warm events than will other regions in higher latitudes, and the large variance of warm events may be attributable to the increase in temperature extreme variability in South Asia (SAS) and Northern Australia (NAU). That is, tropical regions (South Asia (SAS), Indochina, Southeast Asia (SEA), and Northern Australia (NAU)) may possibly be expected to be influenced by more consistent and intense warm extremes, and South Asia (SAS) and Northern Australia (NAU) may be expected to experience increased variability of temperature extremes in the late 21st century under the forcing scenarios.

From projected changes in precipitation extremes, many regions located in South Asia (SAS), East Asia (SEA), Southeast Asia (SEA) and Northern Asia (NAS) are expected to undergo heavy precipitation extremes in the future climate. The fraction of annual high precipitation amounts due to very wet days (R95pTOT) and extremely wet days (R99pTOT) is expected to increase substantially over those regions. This implies that the likelihood of flooding occurrence may possibly be expected to significantly increase in the tropical and sub-tropical areas of the Asia-Pacific (APEC) region.

In examining the ability of all models that participated in IPCC AR4, Alexander et al. (2009) found that no single model is superior or inferior in reproducing the observed trends and patterns in the extremes of temperature and precipitation. Moreover, uncertainty from internal variability of a single climate model is much smaller than that between the different models used in climate change simulations (Deque et al., 2005). Therefore, it is worth noting that the simulation of climate in this study comes from several climate models (four in total), and therefore we may have addressed the systematic errors inherent in the component models. That is, the climate features realized in the trend analysis in this study may be benefited from the elimination of the systematic errors inherent in the individual models. Based

on the findings of this study, the potential influence of climate extremes in a changing climate on communities around the Asia-Pacific region can be better understood. This research is expected to aid future studies working toward the development of an integrated climate-environment-socio-economic system model. Findings from this research are also expected to be practical in establishing an environmental policy for mitigating and adapting to climate change in the Asia-Pacific region. However, further researches are required to assess the uncertainties of climate features in the Asia-Pacific region that are represented by high-resolution models and their ensembles. In addition, the driving mechanisms of regional climate change including extremes in the Asia-Pacific region need to be understood, with a focus on the sources of uncertainty coming from either anthropogenic forcing or natural variability.

Appendix A

The table below shows the name and definitions of a suite of climate change indices developed by the joint World Meteorological Organization Commission for Climatology (CCI)/World Climate Research Programme (WCRP) project on Climate Variability and Predictability (CLIVAR) Expert Team on Climate Change Detection, Monitoring and Indices (ETCCDMI).

Extreme indices related to temperature:

ID	Index name	Index definition	Units
FD	Frost days	Let TN_{ij} be daily minimum temperature on day i in year j. Count the number of days where: $TN_{ij} < 0$°C.	days
SU	Summer days	Let TX_{ij} be daily maximum temperature on day i in year j. Count the number of days where: $TX_{ij} > 25$°C.	days
ID	Icing days	Let TX_{ij} be daily maximum temperature on day i in year j. Count the number of days where: $TX_{ij} < 0$°C.	days
TR	Tropical nights	Let TN_{ij} be daily minimum temperature on day i in year j. Count the number of days where: $TN_{ij} > 20$°C.	days
GSL	Growing season length	Let TG_{ij} be daily mean temperature on day i in year j. Count the number of days between the first occurrence of at least 6 consecutive days with: $TG_{ij} > 5$°C. and the first occurrence after 1st July (1st Jan. in SH) of at least 6 consecutive days with: $TG_{ij} < 5$°C.	days
TX_x	Max Tmax	Let TX_x be the daily maximum temperatures in month k, period j. The maximum daily maximum temperature each month is then: $TX_{xkj} = \max(TX_{xkj})$	℃
TN_x	Max Tmin	Let TN_x be the daily minimum temperatures in month k, period j. The maximum daily minimum temperature each month is then: $TN_{xkj} = \max(TN_{xkj})$	℃
TX_n	Min Tmax	Let TX_n be the daily maximum temperatures in month k, period j. The minimum daily maximum temperature each month is then: $TX_{nkj} = \min(TX_{nkj})$	℃
TN_n	Min Tmin	Let TN_x be the daily minimum temperatures in month k, period j. The maximum daily minimum temperature each month is then: $TN_{xkj} = \max(TN_{xkj})$	℃

ID	Index name	Index definition	Units
TN10p	Cool nights	Let TN_{ij} be the daily minimum temperature on day *i* in period *j* and let $TN_{in}10$ be the calendar day 10^{th} percentile centered on a 5-day window for the base period of 1961-1990. The percentage of time for the base period is determined where: $TN_{ij} < TN_{in}10$	%
TX10p	Cool days	Let TX_{ij} be the daily maximum temperature on day *i* in period *j* and let $TX_{in}10$ be the calendar day 10^{th} percentile centered on a 5-day window for the base period of 1961-1990. The percentage of time for the base period is determined where: $TX_{ij} < TX_{in}10$	%
TN90p	Warm nights	Let TN_{ij} be the daily minimum temperature on day *i* in period *j* and let $TN_{in}90$ be the calendar day 90^{th} percentile centered on a 5-day window for the base period of 1961-1990. The percentage of time for the base period is determined where: $TN_{ij} > TN_{in}90$	%
TX90p	Warm days	Let $TX_{in}90$ be the calendar day 90^{th} percentile centered on a 5-day window for the base period of 1961-1990. The percentage of time for the base period is determined where: $TX_{ij} > TX_{in}90$	%
WSDI	Warm spell duration index	Let TX_{ij} be the daily maximum temperature on day i in period j and let $TX_{in}90$ be the calendar day 90^{th} percentile centered on a 5-day window for the base period of 1961-1990. Then the number of days per period is summed where, in intervals of at least 6 consecutive days: $TX_{ij} > TX_{in}90$	days
CSDI	Cold spell duration index	Let TN_{ij} be the daily minimum temperature on day i in period j and let $TN_{in}10$ be the calendar day 10^{th} percentile centered on a 5-day window for the base period of 1961-1990. Then the number of days per period is summed where, in intervals of at least 6 consecutive days: $TN_{ij} < TN_{in}10$	days
DTR	Diurnal temperature range	Let TX_{ij} and TN_{ij} be the daily maximum and minimum temperature respectively on day *i* in period *j*. If I represents the number of days in *j*, then: $DTRj=\sum(Tx_{ij}-Tn_{ij})/I$	℃

Extreme indices related to precipitation:

ID	Index name	Index definition	Units
Rx1day	Monthly maximum 1-day precipitation amount	Let RR_{ij} be the daily precipitation amount on day *i* in period *j*. The maximum 1-day value for period j are: $Rx1day_j = \max(RR_{ij})$	mm
Rx5day	Monthly maximum consecutive 50day precipitation amount	Let RR_{kj} be the precipitation amount for the 5-day interval ending *k*, period *j*. Then maximum 5-day values for period j are: $Rx5day_j = \max(RR_{kj})$	mm
SDII	Simple precipitation intensity index	Let RR_{wj} be the daily precipitation amount on wet days, $w\ (RR \geq 1mm)$ in period *j*. If W represents number of wet days in *j*, then: $SDII_j = \sum RR_{wj} / W$	mm/ day

ID	Index name	Index definition	Units
R10mm	Number of heavy precipitation days	Let RR_{ij} be the daily precipitation amount on day *i* in period *j*. Count the number of days where: $RR_{ij} \geq$ 10mm	days
R20mm	Number of very heavy precipitation days	Let RR_{ij} be the daily precipitation amount on day *i* in period *j*. Count the number of days where: $RR_{ij} \geq$ 20mm	days
CDD	Consecutive dry days	Let RR_{ij} be the daily precipitation amount on day *i* in period *j*. Count the largest number of consecutive days where: $RR_{ij} <$ 1mm	days
CWD	Consecutive wet days	Let RR_{ij} be the daily precipitation amount on day *i* in period *j*. Count the largest number of consecutive days where: $RR_{ij} \geq$ 1mm	days
R95pTOT	Annual total precipitation in very wet days	Let RR_{wj} be the daily precipitation amount on a wet day w ($RR \geq$ 1.0mm) in period i and let $RR_{wn}95$ be the 95th percentile of precipitation on wet days in the period of 1961-1990. If *W* represents the number of wet days in the period, then: $R95_{pj} = \sum RR_{wj}$ where $RR_{wj} > RR_{wn}95$	mm
R99pTOT	Annual total precipitation in extremely wet days	Let RR_{wj} be the daily precipitation amount on a wet day w ($RR \geq$ 1.0mm) in period i and let $RR_{wn}99$ be the 99th percentile of precipitation on wet days in the period of 1961-1990. If *W* represents the number of wet days in the period, then: $R95_{pj}=\sum RR_{wj}$ where $RR_{wj} > RR_{wn}99$	mm
PRCPTOT	Annutal total precipitation in wet days	Let $RRij$ be the daily precipitation amount on day *i* in period *j*. If *I* represents the number of days in *j*, then: $PRCPTOT_j = \sum(RRij)$	mm

References

Karl, T. R., N. Nicholls, and A. Ghazi, 1999: CLIVAR/GCOS/WMO workshop on indices and indicators for climate extremes: Workshop summary. Climatic Change, 42, 3-7.

Peterson, T. C., and Coauthors: Report on the Activities of the Working Group on Climate Change Detection and Related Rapporteurs 1998-2001. WMO, Rep. WCDMP-47, WMO-TD 1071, Geneva, Switzerland, 143 pp.

REFERENCES

Alexander, L. V., J. M. Arblaster (2009), Assessing trends in observed and modeled climate extremes over Australia in relation to future projections. *Int J Climatol* 29:417-435. doi: 10.1002/joc.1730

Alexander, L. V., X. Zhang, T. C. Peterson, J. Caesar, B. Gleason, A. M. G. Klein Tank, M. Haylock, D. Collins, B. Trewin, F. Rahimzadeh, A. Tagipour, K. Rupa Kumar, J. Revadekar, G. Griffiths, L. Vincent, D. B. Stephenson, J. Burn, E. Aguilar, M. Brunet, M. Taylor, M. New, P. Zhai, M. Rusticussi, and J. L. Vazquez-Aguirre (2006), Global observed changes in daily climate extremes of temperature and precipitation, *J. Geophys. Res.*, 111, doi: 10.1029/2005JD006290.

Braganza, K., D. J. Karoly, J. M. Arblaster (2004), Diurnal temperature range as an index of global climate change during the twentieth century. *Geophys. Res. Lett.*, 31:L13217, doi 10.1029/2004GL019998

Chen, H., J. Sun, X. Chen, W. Zhou (2010), CGCM projections of heavy rainfall events in China. *Int. J. Climatol* doi:10.1002/joc.2278

Choi, G., D. Collins, G. Ren, B. Trewin, M. Baldi, Y. Fukuda, M. Afzaal, T. Pianmana, P. Gomboluudev, P. T. T. Juong, N. Lias, W. T. Kwon, K. O. Boo, Y. M. Cha, Y. Zhou (2009), Changes in means and extreme events of temperature and precipitation in the Asia-Pacific Network region, 1955-2007, *Int. J. Climatol*, 29, 1906-1925.

Coelho, C. A. S., C. A. T. Ferro, D. B. Stephenson, and D. J. Steinskog (2008), Methods for exploring spatial and temporal variability of extreme events in climate data, *J. Climate*, 21, 2072-2092.

Deque, M. R. G. Jones, M. Wild, F. Giogi, J. H. Christensen, D. C. Hassel, P. L. Vidale, B. Rockel, D. Jacob, E. Kjellstrom, M. D. Castro, F. Kucharski, B. V. D. Hurk (2005), Global high resolution versus limited area model climate change projections over Europe: quantifying confidence level from PRODENCE results. *Clim. Dyn.* 25, 653-670. doi: 10.1007/s00382-005-0052-1.

Easterling, D. R., B. Horton, P. D. Jones, T. C. Peterson, T. R. Karl, D. E. Parker, M. J. Salinger, V. Razuvayev, N. Plummer, P. Jamason, C. K, Folland (1997), Maximum and Minimum Temperature Trends for the Globe. *Science*, 227, 364-367.

Easterling, D. R., N. C. Asheville, B. Gleason, K. E. Kunkel, R. J. Stouffer (2007), A comparison of model produced climate extremes with observed and projected trends for the 20th and 21st centuries. The 87th AMS Annual Meeting, AMS Forum: Climate Change Manifested by Changes in Weather. Session 1: Climate and Extreme Weather Events.

Emori, S., S. J. Brown (2005), Dynamic and thermodynamic changes in mean and extreme precipitation under changed climate. *Geophys. Res. Lett*, 32, L17706, doi: 10.1029/2005GL023272

Frich, P., L. V. Alexander, P. Della-Marta, B. Gleason, M. Haylock, A. M. G. Klein Tank, and T. Peterson (2002), Observed coherent changes in climatic extremes during the second half of the twentieth century, *Clim Res.*, 19, 193-212.

Gilbert, R. O. (1987), Statistical methods for environmental pollution monitoring. Van Nostrand Reinhold, New York

Gordon, H. B., L. D. Rotstayn, J. L. McGregor, M. R. Dix, E. A. Kowalczyk, S. P. O'Farrel, L. J. Waterman, A. C. Hirst, S. G. Wilson, M. A. Collier, I. G. Watterson, T. I. Elliott (2002), The CSIRO Mk3 climate system model, Technical Paper No. 60, CSIRO Atmospheric Research, Aspendale, Victoria,

Australia

Hagemann, S., and D. Jocob (2007), Gradient in the climate change signal of European discharge predicted by a multi-model ensemble. *Clim. Change*, 81, 309-327.

Hasumi, H., and Coauthors (2004), K-1 Coupled GCM (MIROC) description. K-1 Model Developers Tech. Rep. 1, 34 pp. [Available online at http://www.ccsr.u-tokyo.ac.jp/kyosei/hasumi/MIROC/tech-repo.pdf.]

Hegerl, G. C., W. Z. Francis, A. S. Peter, V. K, Viatcheslab (2004), Detectability of anthropogenic changes in annual temperature and precipitation extremes. *J. Climate*, 17, 3683-3700.

Houghton, J.T., Y. Ding, D. J. Griggs, M. Noguer, P. J. van der Linden, D. Xiaosu, Eds. (2001), Climate Change 2011: The Scientific Basis. Contribution of Working Group I to the Third Assessment Report of the Intergovernmental Panel on Climate Change (IPCC). Cambridge University Press, Cambridge, UK

Im, E. S., I. W. Jung, D. H. Bae (2011), The temporal and spatial structures of recent and future trends in extreme indices over Korea from a regional climate projection, *Int. J. Climatol*, 31, 72-86.

IPCC (2007a), Climate Change 2007: The Physical Science Basis. Contribution of Working Group I to the Fourth Assessment Report of the IPCC [Solomon, S., D. Qin, M. Manning, Z. Chen, M. Marquis, K. B. Averyt, M. Tignor and H. L. Miller (eds.)]. Cambridge University Press, Cambridge, United Kingdom and New York, NY, USA.

IPCC (2007b), Climate Change 2007: Impacts, Adaptation and Vulnerability. Contribution of Working Group II to the Fourth Assessment Report of the IPCC, M. L. Parry, O. F. Canziani, J. P. Palutikof, P. J. van der Linden and C. E. Hanson, Eds., Cambridge University Press, Cambridge, UK, 976pp.

Kendall, M. G (1975), Rank Correlation Methods. Charles Griffin, London

Kharin, V. V., F. W. Zwiers, X. Zhang, and G. C. Hegerl (2007), Changes in temperature and precipitation extremes in the IPCC ensemble of global coupled model simulation, *J. Climate*, 20, 1419-1444.

Kiktev, D., D. M. H. Sexton, L. Alexander, and C. K. Folland (2003), Comparison of modeled and observed trends in indices of daily climate extremes, *J. Climate*, 16, 3560-3571.

Kioutsioukis, I., D. Melas, and C. Zerefos (2010), Statistical assessment of changes in climate extremes over Greece (1955–2002), *Int. J. Climatol*, 30, 1723–1737.

Klein Tank, A. M. G., and G. P. Können (2003), Trends in indices of daily temperature and precipitation extremes in Europe, 1946-99, *J. Climate*, 16, 3665-3680.

Lynch, A.H., R. D. Brunner (2007) Context and climate change: an integrated assessment for barrow, Alaska. *Climate Change*, 82, 93-111.

Mann, H.B. (1945), Nonparametric tests against trend. Econometrica 13, 245-259

Marengo, J. A., M. Rusticucci, O. Penalba, and M. Renom (2010), An Intercomparison of observed and simulated extreme rainfall and temperature events during the last half of the twentieth century: part 2: historical trends, *Climatic Change*, 98, 509-529.

Meehl, G. A., C. Covey, T. Delworth, M. Latif, B. McAvaney, J. F. B. Mitchell, R. J. Stouffer, and K. E. Taylor (2007), THE WCRP CMIP3 multimodel dataset: a new era in climate change research, *Bull. Am. Meteorol. Soc.*, 88, 1383-1394.

Mao, J., A. Robock (1998), Surface air temperature simulations by AMIP general circulation models: volcanic and ENSO signals and systematic errors. *J Climate*, 11: 1538-1552.

Nakicenovic, N., J. Alcamo, G. Davis, B. de Vries, J. Fenhann, S. Gaffin, K. Gregory, A. Gruebler, T. Y. Jung, T. Kram, E. L. La Rovere, L. Michaelis, S. M. T. Morita, W. Pepper, H. Pitcher, L. Price, K. Riahi, A. Roehrl, H. H. Rogner, A. Sankovski, M. Schlesinger, P. Shukla, S. Smith, R. Swart, S. van Rooijen, N. and Victor, Z. Dadi (2000), Special report on emission scenarios: a special report of working group III of the Intergovernmental Panel on Climate Change, Cambridge University Press, Cambridge, UK.

Peterson, T. C. (2005), Climate change indices, WMO Bulletin, 54, 83-86.

Räisänen, J (2005), Impact of increasing CO2 on monthly-to-annual precipitation extremes: analysis of the CMIP2 experiments. *Clim. Dyn.* 24: 309-323. doi: 10.1007/s00382-004-0510-1

Roeckner, E, G. Bauml, L. Bonaventura, R. Brokopf, M. Esch, M. Giorgetta, S. Hagemann, I. Kirchner, L. Kornblueh, E. Manzini, A. Rhodin, U. Schlese, U. Schulzweida, A. Tompkins (2003), The atmospheric general circulation model ECHAM5. Part I: Model description. Max Plank Institute for Meteorology Rep. 349, 127 pp.

Rusticucci, M., J. Marengo, O. Penalba, and M. Renom (2010), An intercomparison of model-simulated in extreme rainfall and temperature events during the last half of the twentieth century, Part 1: mean values and variability, *Climatic Change*, 98, 493-508.

Sen Roy, S, R. C. Balling (2004), Trends in extreme daily precipitation indices in India. *Int J Climatol* 24:457-466. doi: 10.1002/joc.995.

Shongwe, M. E., G. J. van Oldenborgh, B. J. J. M. van den Hurk, B. de Boer, C. A. S. Coelho, M. K. van Aalst (2009), Projected changes in mean and extreme precipitation in Africa under global warming. Part I: Southern Africa. *J Climate*, 22:3819-3837. doi:10.1175/2009JCLI2327.1.

Sillmann, J, M. Croci-Maspoli (2009), Euro-Atlantic blocking and extreme events in present and future climate simulations. *Geophys Res Lett* 36:L10702. doi:10.1029/2009GL038259.

Sillmann, M., and E. Roeckner (2008), Indices for extreme events in projections of anthropogenic climate change, *Climatic Change*, 86, 83-104.

Stone, D. A., and A. J. Weaver (2002), Daily maximum and minimum temperature trends in a climate model. *Geophys. Res. Lett*, 29:1356. doi: 10.1029/2001GL014556.

Sushama, L, R. Laprise, D. Caya, A. Frigon, M. Slivitzky (2006), Canadian RCM projected climate-change signal and its sensitivity to model errors. *Int. J. Climatol.* 26, 2141-2159.

Tebaldi, C., K. Kayhoe, J. M. Arblaster, and G. A. Meehl (2006), Going to the extremes: an intercomparison of model-simulated historical and future changes in extremes events, *Climatic Change*, 79, 185-211.

Tebaldi, C., and R., Knutti, (2007), The use of multi-model ensemble in probabilistic climate projections. *Philos. Trans. Roy. Soc.*, A365:2053-2075.

Wang, B., I. S. Kang, and J. Y. Lee, 2004: Ensemble simulations of Asian-Autralian monsoon variability by 11 GMs. *J. Clim.*, 17, 803-818.

Yukimoto, S, A. Noda (2002), Improvements of the meteorological research institute global ocean-atmosphere coupled GCM (MRI-CGCM2) and its climate sensitivity. CGER's Supercomputer

Activity Report 10:37-44, NIES, Japan.

Yukimoto, S, A. Noda, A. Kitoh, M. Sugi, Y. Kitamura, M. Hosaka, K. Shibata, S. Maeda, T. Uchiyama (2001), The new meteorological research institute coupled GCM (MRI-CGCM2) - Model climate and variability. *Rap Meteor Geophys* 51:47-88.

Zhang, X, G. Hegerl, F. Zwiers, J. Kenyon (2005), Avoiding inhomogeneity in percentile-based indices of temperature change. *J Climate* 18:1641-1651.

Zhou, L, R. E. Dickinson, A. Dai, P. Dirmeyer (2010), Detection and attribution of anthropogenic forcing to diurnal temperature range changes from 1950 to 1999: comparing multi-model simulations with observation. *Clim Dyn* 35:1289-1307.

APCC TECHNICAL REPORT 2011-03

- Model Evaluation for Low-Level Cloud Feedback
- Evaluation and Future Projection of Changes in Extreme Temperature and Precipitation Events
- Changes in East Asian Winter Monsoon

APEC Climate Center

12, Centum 7-ro, Haeundae-gu, Busan 612-020, Republic of Korea
Tel: +82-51-745-3900 Fax: +82-51-745-3949
www.apcc21.org

비매품
94500
9 788997 533159
ISBN 978-89-97333-18-9
ISBN 978-89-97333-15-8 (세트)